

# Mapping the seismicity of Mars with InSight

Savas Ceylan<sup>1</sup>, Domenico Giardini<sup>2</sup>, John Clinton<sup>3</sup>, Doyeon Kim<sup>2</sup>, Amir Khan<sup>4</sup>, Simon C. Stähler<sup>5</sup>, Géraldine Zenhäusern<sup>6</sup>, Philippe Lognonné<sup>7</sup>, and William Bruce Banerdt<sup>8</sup>

<sup>1</sup>ETH Zurich

<sup>2</sup>ETH Zürich

<sup>3</sup>Swiss Seismological Service

<sup>4</sup>Swiss Federal Institute of Technology

<sup>5</sup>Eidgenössische Technische Hochschule Zürich

<sup>6</sup>Institute of Geophysics, ETH Zurich

<sup>7</sup>Université Paris Cité, Institute de physique de globe de Paris, CNRS

<sup>8</sup>Jet Propulsion Laboratory, California Institute of Technology

March 16, 2023

## Abstract

InSight's seismometers recorded more than 1300 events. Ninety-eight of these, named the low-frequency family, show energy predominantly below 1 Hz down to 0.125 Hz. The Marsquake Service identified seismic phases and computed distances for 42 of these marsquakes, 26 of which have backazimuths. Hence, the locations of the majority of low-frequency family events remain undetermined. Here, we use an envelope shape similarity approach to determine event classes and distances, and introduce an alternative method to estimate the backazimuth. In our similarity approach, we use the highest quality marsquakes with well-constrained distance estimates as templates, including the largest event S1222a, and assign distances to marsquakes with relatively high signal-to-noise ratio based on their similarities to the template events. The resulting enhanced catalog allows us to re-evaluate the seismicity of Mars. We find the Valles Marineris region to be more active than initially perceived, where only a single marsquake (S0976a) had previously been located. We relocated two marsquakes using new backazimuth estimates, which had reported distances of 900, in the SW of the Tharsis region, possibly at Olympus Mons. In addition, two marsquakes with little or no S-wave energy have been located in the NE of the Elysium Bulge. Event epicenters in Cerberus Fossae follow a North-South trend due to uncertainties in location, while the fault system is in the NW-SE direction; therefore, these events are re-projected along the observed fault system.

# Mapping the seismicity of Mars with InSight

S. Ceylan<sup>1</sup>, D. Giardini<sup>1</sup>, J. F. Clinton<sup>2</sup>, D. Kim<sup>1</sup>, A. Khan<sup>1,3</sup>, S. C. Stähler<sup>1,4</sup>,  
G. Zenhäusern<sup>1</sup>, P. Lognonné<sup>5</sup>, W. B. Banerdt<sup>6</sup>

<sup>1</sup>Institute of Geophysics, ETH Zurich, Zurich, Switzerland

<sup>2</sup>Swiss Seismological Service, ETH Zurich, Zurich, Switzerland

<sup>3</sup>Institute of Geochemistry and Petrology, ETH Zurich, Zurich, Switzerland

<sup>4</sup>Physik-Institut, University of Zurich, Zurich, Switzerland

<sup>5</sup>Université Paris Cité, Institut de physique du globe de Paris, CNRS, Paris, France

<sup>6</sup>Jet Propulsion Laboratory, California Institute of Technology, Pasadena, CA, USA

## Key Points:

- We use a similarity analysis to classify noisier seismic events using the high quality marsquakes from InSight as templates
- We relocate marsquakes and update the seismicity map of Mars based on this analysis and new back azimuth estimates
- Our results suggest clusters of seismicity have occurred nearby to Valles Marineris and Olympus Mons

---

Corresponding author: Savas Ceylan, [savas.ceylan@erdw.ethz.ch](mailto:savas.ceylan@erdw.ethz.ch)

**Abstract**

InSight’s seismometers recorded more than 1300 events. Ninety-eight of these, named the low-frequency family, show energy predominantly below 1 Hz down to  $\sim 0.125$  Hz. The Marsquake Service identified seismic phases and computed distances for 42 of these marsquakes, 26 of which have backazimuths. Hence, the locations of the majority of low-frequency family events remain undetermined. Here, we use an envelope shape similarity approach to determine event classes and distances, and introduce an alternative method to estimate the backazimuth. In our similarity approach, we use the highest quality marsquakes with well-constrained distance estimates as templates, including the largest event S1222a, and assign distances to marsquakes with relatively high signal-to-noise ratio based on their similarities to the template events. The resulting enhanced catalog allows us to re-evaluate the seismicity of Mars. We find the Valles Marineris region to be more active than initially perceived, where only a single marsquake (S0976a) had previously been located. We relocated two marsquakes using new backazimuth estimates, which had reported distances of  $\sim 90^\circ$ , in the SW of the Tharsis region, possibly at Olympus Mons. In addition, two marsquakes with little or no S-wave energy have been located in the NE of the Elysium Bulge. Event epicenters in Cerberus Fossae follow a North-South trend due to uncertainties in location, while the fault system is in the NW-SE direction; therefore, these events are re-projected along the observed fault system.

**Plain Language Summary**

InSight’s seismometer recorded more than 1300 events since landing on the surface of Mars in November 2018 until it retired in December 2022. Most of the events InSight recorded are at high frequencies  $\geq 2.4$  Hz. The rest of the events, named the low-frequency family, produce signals that travel through the planet’s interior, allowing us to understand the interior structure when event locations can be determined using seismic arrivals. However, marsquakes are often weak and do not always exhibit clear seismic phases; therefore, they cannot be assigned distances using traditional techniques. Here, we use the well-understood, highest-quality events as templates to investigate and assign a source region to the weaker seismic signals. Seismicity on Mars occurs mostly along or north of the boundary between the southern highlands and northern lowlands. Valles Marineris is seismically more active than previous catalogs of located events imply. Further, we show evidence that two events likely originate from the Olympus Mons region.

**1 Introduction**

The Mars InSight mission (Banerdt et al., 2020) retired on December 21, 2022, after more than four years (1446 sols or Martian days) of successful operations. The mission deployed the first seismic station (SEIS) on the surface of the planet, comprising both a very broadband (VBB) and a short-period (SP) seismometer (Lognonné et al., 2019; Lognonné et al., 2020). The InSight payload also contained wind and pressure sensors for observing the Martian atmosphere (Banfield et al., 2020), which provided crucial information for discriminating seismic events from environmental noise sources; the HP<sup>3</sup> temperature probe (Spohn et al., 2022); and the robotic arm and cameras used for deploying SEIS and HP<sup>3</sup> on the ground (Banerdt et al., 2020).

Throughout the mission, the Marsquake Service (MQS; Clinton et al., 2018) cataloged more than 1300 signals of seismic origin (Table S1; InSight Marsquake Service, 2023) in the exceptionally high-quality and complete waveform dataset (Clinton et al., 2021; Ceylan et al., 2022). Ninety-eight of these events are part of the low-frequency (LF) event family showing energy predominantly below 1 Hz. The rest of the events contain energy mostly above 2.4 Hz and are classified as the high-frequency (HF) family.

For events in the LF family, when seismic phases can be identified (typically direct P and S, or their surface reflections PP and SS for distant events  $\gtrsim 100^\circ$ ), MQS determines event distances using the theoretical travel times from the model set of Stähler et al. (2021) following the single station location algorithm described in Khan et al. (2016) and Böse et al. (2017). The location of an event is obtained when a backazimuth can also be reliably determined (Böse et al., 2017); in current MQS practice, this follows the method described in Zenhäusern et al. (2022) since V12 catalog (InSight Marsquake Service, 2022).

In the V14 catalog, MQS computed distances for 42 of the 98 LF family events (Figure 1a). Twenty-four of these events are fully located with a backazimuth (hence assigned quality A), while the remaining events only have a distance estimate and are quality B or C (Table S1). The vast majority of the fully-located events cluster at distances between  $25^\circ$  and  $35^\circ$  with a backazimuth towards the East, pointing to the Cerberus Fossae region (Figure 1a).

The most distant marsquake (S0976a; Figure 1) was observed on August 25, 2021, at a distance of  $146 \pm 7^\circ$  from InSight and a backazimuth of  $101 \pm 25^\circ$ , locating the event in the Valles Marineris region (Horleston et al., 2022). Two events (S1000a and S1094b; hereinafter, referred to as S1000<sup>I</sup> and S1094b<sup>I</sup> for brevity) showed the first clear indication of seismic surface wave arrivals (Kim et al., 2022). Both of these events were later confirmed as distant impacts (Posiolova et al., 2022) with Mars-calibrated moment magnitudes (Böse et al., 2018) of  $M_W^{Ma} 4.0 \pm 0.2$  and  $4.1 \pm 0.2$  (Figure S1) and crater diameters of 130 and 150 m, respectively. Furthermore, six HF family events within 300 km of InSight have also been confirmed as impacts (Garcia et al., 2022; Daubar et al., 2023), which show dispersive acoustic signals propagating along a waveguide in the form of chirps in their coda, with strong linear polarization pointing toward the source. Finally, the largest marsquake ( $M_W^{Ma} 4.6 \pm 0.3$ ) recorded by InSight is S1222a (Kawamura et al., 2023), which occurred on May 4, 2022 (Figure S1).

Giardini et al. (2020) and Lognonné et al. (2020) give the first interpretations of the global seismicity on Mars and interior structure using limited number of both HF and LF family events recorded during the first year of the mission. Subsequently, body waves have been successfully utilized for studying the crust beneath the lander (Knapmeyer-Endrun et al., 2021; Kim, Lekic, et al., 2021; Li et al., 2022; Durán, Khan, Ceylan, Zenhäusern, et al., 2022), Martian mantle (Khan et al., 2021; Durán, Khan, Ceylan, Zenhäusern, et al., 2022; Durán, Khan, Ceylan, Charalambous, et al., 2022; Khan et al., 2022) and core (Stähler et al., 2021; Durán, Khan, Ceylan, Zenhäusern, et al., 2022; Khan et al., 2022; Irving et al., 2022). Kim et al. (2022) obtained the average crustal velocity structure along the minor-arc paths using Rayleigh waves observed in S1000a<sup>I</sup> and S1094b<sup>I</sup> (Posiolova et al., 2022). Most recently, surface wave studies of S1222a enabled us to further understand crustal anisotropy by using fundamental-mode Rayleigh and Love waves (Beghein et al., 2022) and together with their overtones (Kim et al., 2023). In the same record, Rayleigh waves that orbit around Mars have been also detected and used for estimating the planet’s average crustal thickness (Kim & et al., 2023).

The large number of noisy events is not surprising, since marsquakes are low-amplitude and the background seismic noise at InSight is highly variable. Interpreting these noisier events without any distance estimate is challenging. In order to overcome this limitation, Giardini et al. (2020) introduced an alignment-based methodology where the weak marsquakes are assigned a distance depending on their similarities with the highest-quality events whose distances were assumed fixed or anchored. In their approach, the events are visually aligned based on the predicted travel times of seismic phases using an interior reference model. Since V3 catalog (InSight Marsquake Service, 2020), MQS adopted this visual alignment approach in their locations as an alternative to interpret the events using a recent reference model from Stähler et al. (2021).

While the structural studies thus far have used the events with the highest signal-to-noise (SNR) ratio, the vast majority of the seismic events and their waveform characteristics (e.g., secondary arrivals in the signal coda and high-frequency content of some LF family events) remain to be understood. Here, we extend the visual alignment approach by introducing the Dynamic Time Warping algorithm (Sakoe & Chiba, 1978), and apply it to a larger set of LF family events now available. We first classify the relatively weaker signals using the events with the highest SNR ratio as templates. Then, we re-evaluate the seismicity on Mars in light of similarities and known tectonic regions.

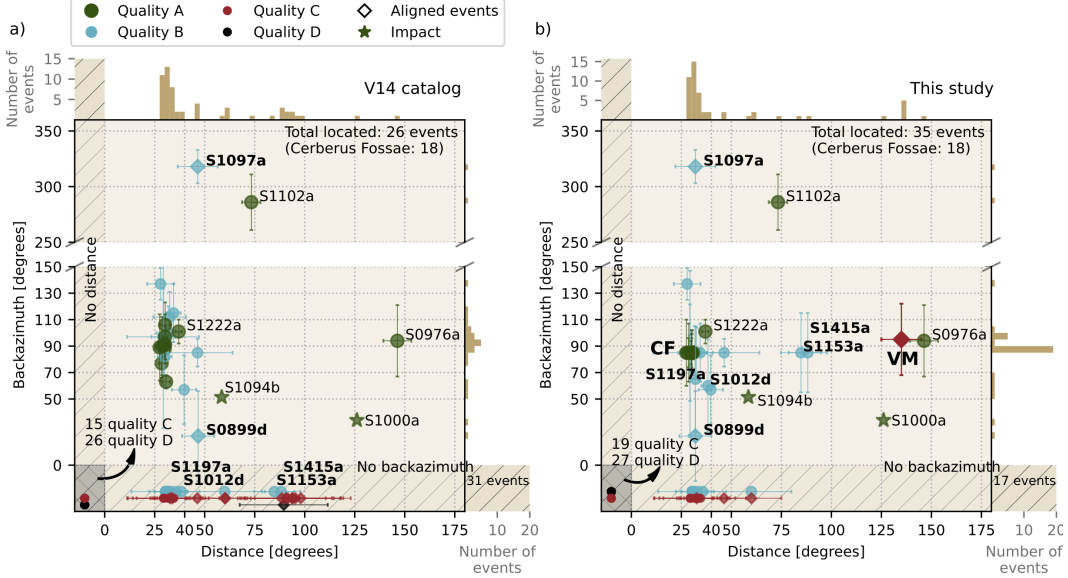


**Figure 1.** Distance and backazimuth distribution of the LF-family events in (a) the V14 catalog (InSight Marsquake Service, 2023), and (b) this study. The confirmed impacts, S1000a<sup>I</sup> and S1094b<sup>I</sup>, are denoted by stars. The 6 events labelled in bold-face have locations that are newly introduced or are modified in this study. Note a number of events without back azimuths also have their distances revised. Diamonds indicate events in V14 where the distance is only provided by visual alignments. The colors and marker sizes show the event qualities as indicated in Table S1. The histograms indicate the number of events for distance (top) and backazimuth (right). A majority of the catalog includes events at distances around 30° and a backazimuth towards East (80–100°), pointing to the Cerberus Fossae region. The hatched regions show events without backazimuth or distance estimates. The errors bars show the uncertainties in distance and backazimuth. See Figure S1 for the distance and  $M_W^{Ma}$  distributions, and Table S2 for a summary of re-evaluated events and our modifications. CF: Cerberus Fossae, VM: Valles Marineris.

## 2 Data and methods

For our analysis, we use spectral envelopes derived from the 20 samples-per-second (sps) VBB waveform data from the LF family events cataloged during the entire mission. All the events and waveforms (InSight Mars SEIS Data Service, 2019b, 2019a) are publicly available with the release of the V14 catalog (InSight Marsquake Service, 2023). A breakdown of the catalog, including the HF events, is provided in Table S1.

Our method builds on the visual alignment approach of Giardini et al. (2020). In the visual alignments, event envelopes of both low SNR events and high quality are com-

pared, and weaker events are assigned a relative distance using the envelope similarities, theoretical travel time curves and the events with pick-based distances as anchors. However, the low SNR events are often found to be similar to multiple template events, i.e., in the shape and length of their S-wave coda. Consequently, interpretation of events is often challenging and ambiguous.

In order to address these particular cases, we introduce the dynamic time warping (DTW; Sakoe & Chiba, 1978) algorithm to measure event similarity using the shape of their spectral envelopes (Figures 2 and 3). Additionally, we use an alternative approach to determine new backazimuths for a subset of events using a grid search for the waveform envelopes, as illustrated in Figure 4. Finally, we provide distances for the events with lower SNR by finding the best matches to the collection of high-quality template events, with addition insights from backazimuths in some cases, and separate the seismicity into classes (Figure 5). Our analysis assumes the source and structural effects along the propagation path, such as attenuation and scattering, are negligible.

## 2.1 Similarity analysis

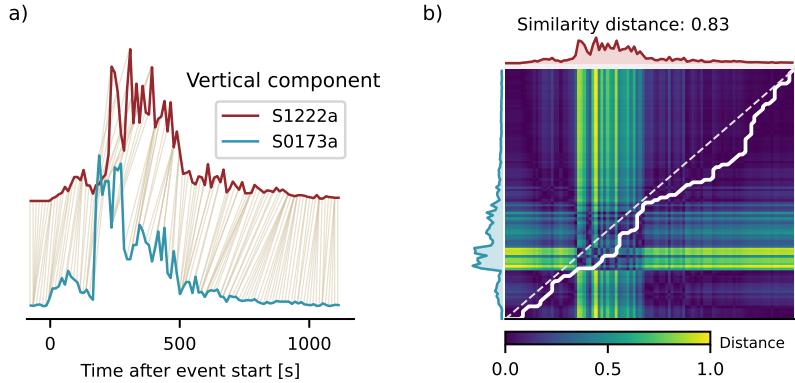


**Figure 2.** Example of the DTW method (Sakoe & Chiba, 1978) to determine the shape similarity between the spectral envelopes of two of the high-quality marsquakes, S1222a and S0173a. (a) The final optimal point-wise pairings between the event envelopes. The light-brown lines indicate matching data points with minimum distance in  $\|L_1\|$  norm. (b) The warping path and cross-similarity matrix. The color bar shows the normalized distance measure for similarity, with larger values indicating less similarity. The warping path would be perfectly diagonal (dashed line) if the envelopes were identical. The deviation from the ideal path for these two events is reasonably close to the diagonal.

The data processing workflow we use to generate envelopes is summarized in Figure S2. First, we remove the instrument response to obtain acceleration time series and rotate the VBB data into the ZNE (vertical-North-East) coordinate frame. Then, we compute spectrograms for all three components using a window length of 30 s and an overlap of 60%. Finally, we obtain the envelopes by summing the spectral amplitudes in power for each component in linear scale along the frequency axis between 0.25 and 0.9 Hz, which is a frequency window that is rich in energy for the majority of LF family events (Ceylan et al., 2022). The upper bound is intentionally below 1 Hz to avoid an artifact caused by the electronics (Zweifel et al., 2021). The envelopes have a sample point every 12 seconds. Although different parameters in terms of physical units, window lengths and overlaps can be used, the selected parameters are preferred through experience gathered throughout the mission so as to allow for comparison of events from different distances. We use

the vertical component for measuring envelope similarities since it is the least-contaminated by atmospheric disturbances.

For data regularization in advance of the DTW (Figures 2 and 3), a short time-window around significant glitches in the time series are masked in the spectral envelopes. Glitches are ubiquitous artifacts observed in the data (Scholz et al., 2020; Ceylan et al., 2021) and may lead to inaccurate interpretations (Kim, Davis, et al., 2021). For masking, we replace the original envelope values with the mean of adjacent data points. The glitch windows have been manually identified by the MQS. The spectral envelopes start 90 s prior to the energy onset as marked in the V14 catalog. The end times are manually assigned for the few events that have a very long duration ( $>1\text{h}$ ); otherwise, we use the signal end from the catalog (InSight Marsquake Service, 2023). For similarity metrics, the point-wise distances in Figure 2a are computed using the  $\|L_1\|$  norm because of its stability and relative insensitivity to noisy time series. The final similarity values (Figure S3) are normalized with the warping path length to account for differences in the duration of the time series.

The DTW method is not suitable to use in an automated style for our purposes. For instance, an event with no apparent S-wave energy may show a relatively higher degree of similarity to another event with strong S-wave (e.g., S1097a and S0235b in Figure 3a and b). Therefore, an a-priori knowledge of events for their available phase picks, polarization attributes and P- and S-wave coda lengths are required for interpretation.

## 2.2 Backazimuth estimation

Backazimuth is defined as the angle between the seismic station and epicenter with respect to North in a station-centric coordinate frame. MQS initially determined backazimuth from the 3-component particle motions in the time domain (Böse et al., 2017), though recently migrated to a more rigorous approach using polarization measured using both P and S-wave arrivals in the frequency-time domain (Zenhäusern et al., 2022). MQS does not assign backazimuths when the results from either method are interpreted to be unstable.

In an attempt to increase the number of events with assigned backazimuths, we adopt a grid search method using the envelope timeseries. A variation of this approach has been successfully applied to determine the backazimuth of the HF events in Stähler et al. (2022). Here, using well documented events, we demonstrate that our approach can recover similar backazimuths to other methods. Figures 4 and S4–S6 show how this approach performs for the 2 distant impacts as well as the large events S0235b and S1222a.

In order to find the most plausible rotation angle range, we rotate the spectral envelopes for  $360^\circ$  with an increment of  $2^\circ$ . Ideally, in the presence of P-waves, the energy ratio of vertical (Z) and radial (R) components compared to the transverse (T) must be maximized when the rotation is in the same direction as the true backazimuth. As a reliability check, the transverse-to-radial ratio should have maxima at  $90^\circ$  perpendicular to the vertical-to-transverse component ratio. In our test cases, the cross-power of Z and R components ( $Z.R/T$ ) better accentuates the results (Figure 4c, S4-S6), which makes picking backazimuths easier. We choose the backazimuth values using the first concentrated amplitude ratios in the time window directly after the initial phase arrivals and assign the uncertainties visually. Since we only use envelope amplitudes, we cannot eliminate the  $180^\circ$  ambiguity (Figure 4).

## 3 Results and discussion

The InSight seismicity catalog (Clinton et al., 2021; Ceylan et al., 2022) is a collective inventory of work from the InSight science team that includes not only the lo-

cations provided by MQS, but also locations of known impacts (Posiolova et al., 2022; Garcia et al., 2022), alternative source interpretations (Kedar et al., 2021), seismic phase picks (e.g. Khan et al., 2021; Stähler et al., 2021; Durán, Khan, Ceylan, Zenhäusern, et al., 2022), and distance and seismic phase assignments from the visual alignments (Giardini et al., 2020). Our analysis below provides new, updated alignments that allows us to assign distances to substantially more of the LF family of events, coral events into classes or group, enabling us to re-evaluate our understanding of Martian seismicity. A summary of the work is shown in Figure 5, where the various event groups are present in terms of their distance from the InSight lander. These results can be expected to included in final, post-mission catalog releases from MQS.

The map of the seismicity of Mars as contained in the MQS V14 catalog (InSight Marsquake Service, 2023) is summarized in Figure 6a, while our interpretation resulting from this analysis is in Figure 6b (also see Figures S10–S12 for each class discussed below). The seismicity on Mars appears to occur along or to the North of the dichotomy boundary. Furthermore, it is notable that 2 of the 3 template events from distances  $>90^\circ$  are the S1000a<sup>I</sup> and S1094b<sup>I</sup> impacts.

### 3.1 Distant events cluster

The so-called distant events (Figure 7) are a class of seismic signals that are bound between the 2 most distant template events, S1000<sup>I</sup> and S0976a. The low SNR signals that match this group lack any indication of P-energy and exhibit relatively long energy packages, which we interpret as S-wave coda. The visual alignments placed these events at distances  $>90^\circ$  using the length of the S-wave coda as a proxy for distance (Figures 6a and S11). The two distant template events, the only ones to lie beyond the core shadow, did not occur until late in the mission over 2.5 years after landing. Therefore, although the weak events now assigned at this distance occurred early on the mission, there was no possibility to constrain their event distances until recently.

MQS locates S0976a in the Valles Marineris region (Horleston et al., 2022),  $146\pm 7^\circ$  away from InSight. S1000a<sup>I</sup> occurred in Tempe Terra at a distance of  $126^\circ$  (Figure 6a) (Posiolova et al., 2022). In this context, we note that an independent joint seismic event-location and structure-inversion scheme predicts a location for S1000a<sup>I</sup> in excellent agreement with the imaged location (Durán, Khan, Ceylan, Zenhäusern, et al., 2022). The length of the S-wave coda for distant events is more comparable to S1000a<sup>I</sup> as it is shorter than S0976a (Figures 5 and 7), suggesting that these events occurred at a distance range of  $\sim 130\text{--}140^\circ$ , possibly closer to S1000a<sup>I</sup>.

Considering the lack of any energy that we interpret to be P-wave, as well as the emergent nature of the S-energy, the envelope-based back azimuth approach was not used to try further constrain locations for these events. The only evidence of tectonic-related seismic activity at these distances is from Valles Marineris. Valles Marineris is one of the largest canyons in the whole Solar system (Coles et al., 2019) and has been proposed as one of the most plausible candidates to produce marsquakes, using both surface faulting observations (Golombek et al., 1992) and joint inversion of gravity and topography data (Gudkova et al., 2017). It is reasonable to assume that the region is more active than might be suggested on account of the observation of a single event. Therefore, we assign these events a distance of  $130\text{--}140^\circ$ , and suggest that the source region could be in the western part of Valles Marineris (Figure 6b and d).

### 3.2 Assigning locations to S1153a and S1415a

In V14 catalog, MQS provides only distance estimates for S1153a and S1415a at  $84.8\pm 10^\circ$  and  $88.2\pm 9.6^\circ$ , respectively. In addition to being the only events in the catalog with phase-based distances at this distance, the frequency content of the events are

also remarkably similar (Figure S8). Furthermore, they show a high degree of similarity in all three components (Figures 8a and S7), suggesting that most likely both events originated from the same region.

MQS does not assign a backazimuth to either of these events due to their emergent P-arrivals and contaminated waveform characteristics (Figure S8). Applying the envelope-based grid search approach for S1153a, we obtain a backazimuth estimate of  $85\pm 30^\circ$  with the  $180^\circ$  ambiguity (Figure 8a), which places the event in a region SW of Olympus Mons. A reliable backazimuth pick was not possible for S1415a, although the P-wave energy partitioning between the horizontal components imply a value similar to S1153a in a more NE-SW direction (Figure 8b). Considering the large uncertainties for S1153a, we assume both events occurred roughly in the same region and locate them SW of Olympus Mons (Figure 6b and S10).

It is noted that in the V14 catalog and seen in Figure 1a, there is a cluster of aligned events assigned also to this distance. As described in the previous subsection, all these aligned events have been moved further away from InSight to Valles Marineris.

### 3.3 Events near to S1094b<sup>I</sup>: S0185a and S0234c

The S1094b<sup>I</sup> impact crater was detected in Amazonis Planitia at a distance of  $58.5^\circ$  with a backazimuth of  $51.4^\circ$ . Two relatively weak events S0185a and S0234c are shown to have strong similarity, as demonstrated in Figures 9 and S7b. The distance for S0185a is calculated by MQS as  $60\pm 20^\circ$ . S0234c is assigned a distance of around  $70^\circ$  through visual alignment. Neither of the events have MQS assigned backazimuths. Our similarity metrics confirm that S1094b<sup>I</sup> is very similar to S0185a, and similar to S0234c (Figure S7). Therefore, we do not modify the previously reported distances.

No reliable backazimuth for either S0185a and S0234c can be obtained from our envelope-based grid search approach. The closest seismic event with a location is S1102a ( $73.3\pm 5^\circ$ ), located in Syrtis Major Planum (Figure 6), though this event is  $20^\circ$  further out. The MQS distances for S0185a and S0234c coincide well with the eastern portion of Syrtis Major Planum; however, it is difficult to assign a specific source region without any indication of backazimuth for either of the events.

### 3.4 Events similar to S0899d: marsquakes with weak or no S-waves

S0899d has a strong arrival that can clearly be associated to a P-wave via its vertical polarization which indicates that the event comes from a direction to the North of InSight with a backazimuth of  $22\pm 30^\circ$  (Table 1, Figure 6). A subset of weak marsquakes, like S0899d, also show little-to-no S-wave energy (Figure 10) in the vertical component or have an S-to-P ratio  $\sim 1$ . The template for this class of events is S0899d, which does not have a pick-based location, although visual alignments suggest a distance of  $\sim 46^\circ$  due to its similarity to S0183a.

Here, using the envelopes, we identify for the first time S-wave arrivals for S0899d and S1097a on the horizontal components (Figure 10), and modify their aligned distances from  $46^\circ$  to  $32^\circ$  by aligning the event against the theoretical travel times from the reference model (Figures 5 and 6). S0183a remains an outlier: although the event clusters with S0899d in terms of envelope characteristics, its epicenter in the V14 catalog is at a distance of  $46^\circ$  (Figure 6). Khan et al. (2021) provides an alternative distance range and locates S0183a at  $54\text{--}59^\circ$  using differential arrival times of seismic phases from multiple events and the current knowledge of mineralogy.

S1012d and S1197a were not assigned a backazimuth in V14. Using the envelope grid search method, we propose that the events have backazimuths of  $60\pm 35^\circ$  and  $65\pm 40^\circ$ , respectively (Figure 11). This means the events locate close to S0325a, so there is now

a cluster of three events in this class (Figures 6 and S11). Due to the  $180^\circ$  ambiguity, it is possible that these events are on the opposite side of the azimuth semicircle. However, the observed seismicity on Mars appears to occur along or North of the equatorial dichotomy (Figure 6); therefore, we find our preferred backazimuth more plausible.

The tectonic source behind this event class has yet to be discovered. Giardini et al. (2020) and Khan et al. (2021) explain the lack of S-waves with distance and suggest that S-waves are attenuated between  $\sim 40\text{-}60^\circ$  where seismic waves propagate through a low-velocity layer in the mantle. With more data available, the epicenters determined by MQS and our re-locations imply a scattered and closer distribution of these events; hence, distance alone cannot explain the lack of S-waves. We cannot assign a single region for these events; therefore, we attribute the decrease in S-wave energy to geometrical spreading due to strong 3D mantle structure or an S-wave low velocity layer in the lithosphere (Giardini et al., 2020; Khan et al., 2021), or source mechanism.

**Table 1.** Location parameters of S0899d class. The V14 distances with asterisks are assigned using the visual alignment rather than phase picks. We modified the previously assigned distances for S0899d and S1097a using new S-picks on Figure 7, and calculated new backazimuths for S1197a and S1012d (Figure 11). BAZ: backazimuth.

Event name	V14 Distance ( $^\circ$ )	V14 BAZ ( $^\circ$ )	This study Distance ( $^\circ$ )	This study BAZ ( $^\circ$ )
S0183a	$46.0\pm 17.0$	$85\pm 17$	–	–
S0899d	$46.7\pm 10^*$	$22\pm 30$	$32\pm 10$	–
S1197a	$32.0\pm 1.5$	–	–	$65\pm 40$
S1097a	$46.2\pm 10^*$	$318\pm 20$	$32\pm 10$	–
S1012d	$38.2\pm 3.3$	–	–	$60\pm 35$
S0325a	$39.7\pm 6.1$	$57\pm 20$	–	–

### 3.5 S1222a and the Cerberus Fossae class

S1222a, which occurred on May 4, 2022, is the largest event ( $M_W^{Ma} 4.6\pm 0.2$ ) recorded since landing. The event is  $37^\circ\pm 1.6$  away from InSight, and unlike most of the LF family, shows clear Rayleigh and Love waves including their overtones. The MQS backazimuth estimate for S1222a is  $101\pm 8^\circ$  (Kawamura et al., 2023), while using the envelope-based approach we obtain  $125^\circ\pm 15$  which is also consistent with the direction of propagation from the minor-arc surface waves (Kim et al., 2023). This suggests that the event perhaps originated closer to the Martian dichotomy boundary (Andrews-Hanna et al., 2008) than the location reported in V14 catalog. Interestingly, although the event did not originate in the Cerberus Fossae, we observe that the S1222a envelopes are largely similar to those of the LF events with excess energy in the S-wave coda from Cerberus Fossae (Figure 2 and 12).

InSight did not record any tectonic events closer than  $25^\circ$  from the station (Figure 1a). A large number of the LF-family events, which show relatively clear P- and S-wave arrivals, are located in the Cerberus Fossae region,  $25\text{--}35^\circ$  away from the station due East (Durán, Khan, Ceylan, Zenhäusern, et al., 2022; Stähler et al., 2022). Within this cluster of events, the decay of P- and S-wave coda is similar, although some events show excess energy in their coda (e.g. S0173a vs S0235b; Figure S9). No new events were added to this cluster class though our study.

Stähler et al. (2022) attributes the seismicity in the Cerberus region to the active deformation caused by recent volcanism. The authors also show that the HF events come

from a similar direction as the LF family events located in the region and propose that all HF events originate from the central part of Cerberus Fossae in the form of very shallow events associated with large active volcanic dykes.

The strike of the Cerberus Fossae fault system is directed NW-SE (yellow lines in Figures 6c and S13), while the epicenters of Cerberus events follow an N-S trend. In order to be consistent with the surface observations (Knapmeyer et al., 2006; Perrin et al., 2022), we project all Cerberus events to the center of the fault system while maintaining their reported distances.

## 4 Conclusions

Contrary to pre-mission expectation (Knapmeyer et al., 2006), we find that over the lifetime of the mission, InSight did not observe a wide distribution of seismicity across the planet. Except for S1222a, seismicity was not observed on wrinkle ridges. Instead, the seismicity appears to focus on isolated tectonic features in a few distance ranges and locations along or North of the Martian dichotomy (Figure 6), implying that contraction due to cooling is not the dominant driver of present-day Martian tectonics, as proposed for other smaller terrestrial planets, Mercury and the Moon (Byrne et al., 2014):

- (i) A number of low SNR events that due to their very long duration are likely distant events and were originally located by visual alignments at distances  $>90^\circ$ , are found to be highly similar to the impact event S1000a<sup>I</sup> at  $126^\circ$  away from InSight. In light of the only evidence of a tectonic region at these distances from S0976a, these events are likely to occur in southern Tharsis region, plausibly in western Valles Marineris (Figure 6b and d). The absence of observed seismicity from the heavily faulted Tharsis region had been puzzling beforehand, but can now be explained by the fact that SS and PP waves from these distances are generally highly scattered and can only be identified as such by comparison to template events such as the S1000a<sup>I</sup>.
- (ii) Two events (S1153a and S1415a) have similar envelope shape (Figure 8b) and spectral content (Figure S2). These events have distances around  $90^\circ$  as computed by MQS. We find a backazimuth of  $85^\circ$  for S1153a (Figure 8a), and locate both of these events in the approximate area of Olympus Mons (Figure 6), which is surrounded by a basal scarp of 2–10 km height and thrust faults as young as  $<40\text{Ma}$  (Weller, 2015).
- (iii) S0185a and S0234c can be paired with the impact S1094b<sup>I</sup>. The event distances are compatible with a source region at a distance of  $\sim 60^\circ$  (Figure 5 and 9); however, since S0185a and S0234c have no convincing indication of backazimuth, we are not able to identify a single source region.
- (iv) A subset of events (S0899d class) show little or no S-wave energy, specifically on the vertical component (Figure 5). We computed backazimuths for two of the events in this class (S1012d, S1197a; Figure 11). This class of events shows no spatial clustering; therefore, the source region is unknown. The lack of stronger S-waves remains puzzling. Possible reasons are source mechanism, geometrical spreading due to strong 3D mantle structure or a relatively thin S-wave low velocity zone due to a velocity inversion in the lithosphere (Khan et al., 2021).
- (v) The main seismogenic region on InSight’s hemisphere of Mars (Figure 1) remains to be the central part of Cerberus Fossae (InSight Marsquake Service, 2023; Stähler et al., 2022), with original MQS epicenters aligned in a N-S trend (Figure 6a and c). Since the faults in the region have a strike along NW-SE direction (Perrin et al., 2022), we re-assign those events to the center of the Cerberus Fault system.

Our re-locations have no effect on the recent interior models (e.g. Khan et al., 2021; Stähler et al., 2021; Kim et al., 2022) since we do not adjust the locations or seismic phase

picks for the high-quality events. However, our re-evaluations of e.g., the distant event class, are potentially important for future studies aiming at the deep interior of Mars (e.g. Irving et al., 2022), as well as regional seismicity and global stress field estimates of the planet (e.g. Knapmeyer et al., 2023).

## 5 Open Research

The waveform data and seismicity catalog are available from InSight Mars SEIS Data Service (2019a) and InSight Mars SEIS Data Service (2019b). The InSight seismicity catalog is from InSight Marsquake Service (2023). We used the ObsPy (Krischer et al., 2015), NumPy (Harris et al., 2020) and scipy (Virtanen et al., 2020) packages for data processing. We benefited from the tslearn package of Tavenard et al. (2020) for similarity analysis.

## Acknowledgments

We acknowledge NASA, CNES, partner agencies and institutions (UKSA, SSO, DLR, JPL, IPGP-CNRS, ETHZ, ICL, MPS-MPG), and the operators of JPL, SISMOC, MSDS, IRISDMC and PDS for providing the SEIS data. Marsquake Service (MQS) operations at ETH are supported by ETH Research grant ETH-06 17-02. The authors recognise support from the ETH+ funding scheme (ETH+02 19-1: “Planet Mars”). This is InSight Contribution Number 195.

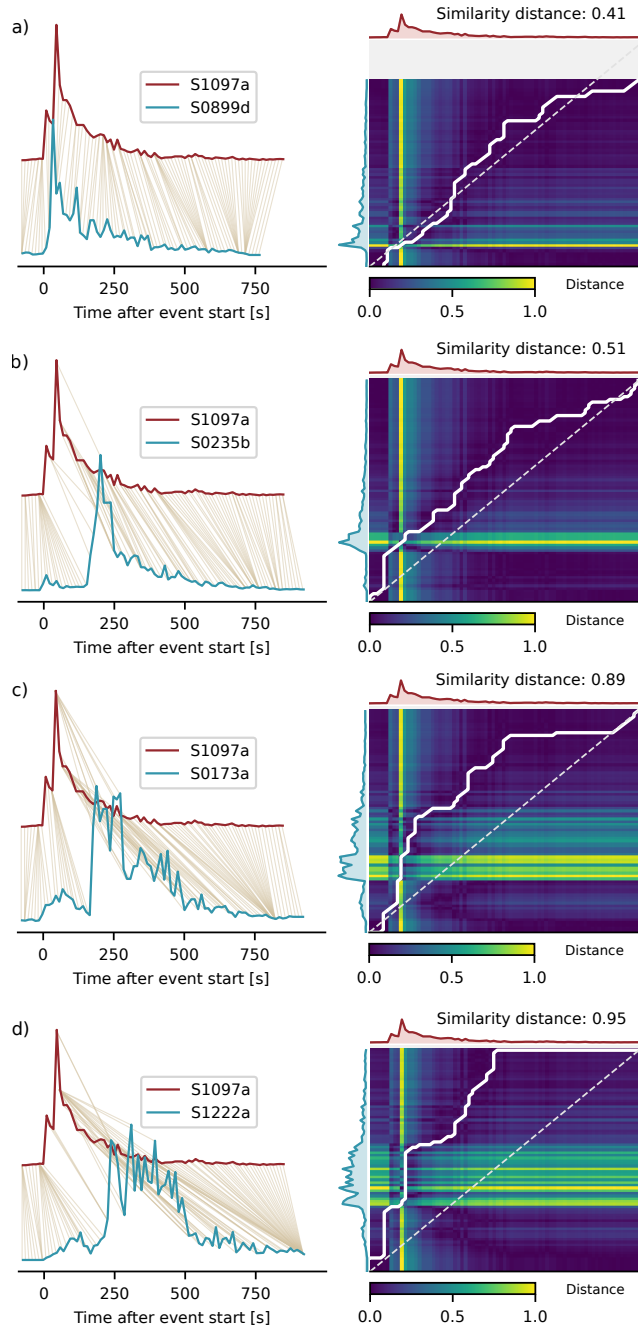


**Figure 3.** Similarity analysis for S1097a, an LF QB event without an assigned distance in the V14 catalog, against 4 template events. The final similarity distances in  $\|L_1\|$  norm are indicated in the warping path panels, where smaller values indicate higher level of similarity (Figure S3). The event is most similar to S0899d (a), another LF QB event without a pick-based distance in the catalog. Therefore, S1097a clusters within the same class. Note that the envelope shape is also significantly similar to S-wave coda of S0235b (b). The degree of similarity decreases for other templates in (c) and (d).

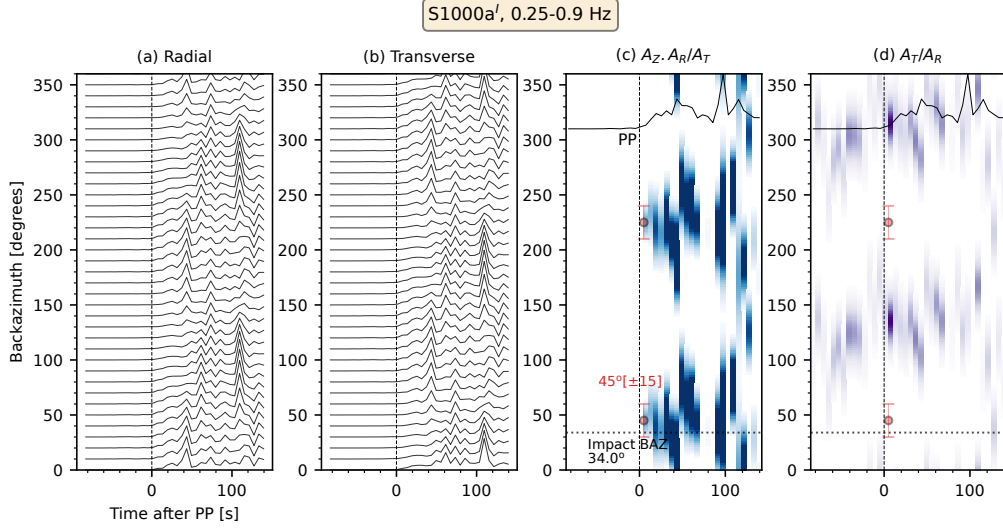


**Figure 4.** Validation of envelope-based grid search approach for backazimuth estimation using S1000a<sup>I</sup>. The impact crater (Posiolova et al., 2022) is detected 126.09° away from InSight and at a backazimuth of 34° (Posiolova et al., 2022). The vertical dotted lines at zero time on each panel indicate the PP phase arrival time. (a) and (b) show the rotated horizontal envelopes, computed for frequencies between 0.25 and 0.9 Hz. The envelope amplitudes are normalized using the maximum of the vertical component for visualization purposes. (c) and (d) denote combined vertical (Z) and radial (R) to transverse (T) and T/R ratio, respectively. The orange circles and error bars show the preferred backazimuth pick with the ambiguity, computed using envelope amplitudes prior to normalization. For reference, the Z-component envelopes are plotted at the top of (c) and (d). The horizontal dotted lines in (c) and (d) show the true backazimuth. The color scale in (c) is saturated to make the amplitudes after the PP more visible.

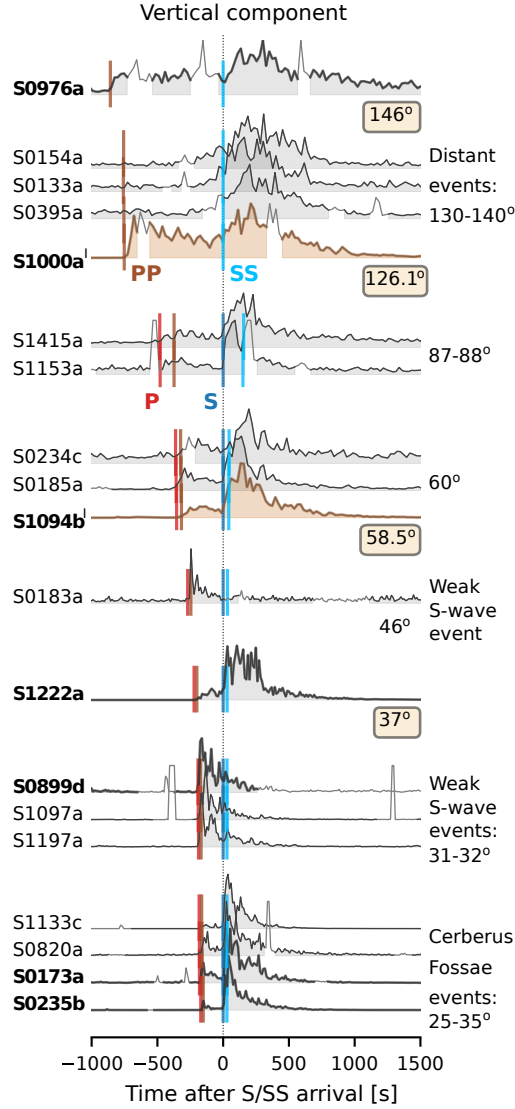


**Figure 5.** Overview of event classes. Each class is indicated by the label on the right. Template events are indicated by bold lines and font. Timeseries show the envelopes computed from vertical component acceleration data for frequencies 0.25–0.9 Hz. The light-gray parts of the envelopes show the unglitched data, note the glitches are masked for similarity processing. The 2 envelopes in a tan color are the known impacts. The distances from V14 are indicated on the right side for all template events outside of the Cerberus Fossae cluster. The zero time is the first arriving theoretical S-wave (S or SS depending on the distance) from a reference model (Stähler et al., 2021; Ceylan et al., 2022). Theoretical arrival times for P, S, PP and SS phases are marked and labelled. S0899d, S1097a and S1197a belong to the same class with S0183a, but clearly lie closer to InSight at around  $32^\circ$ . Envelopes are in log-scale to emphasize similarities at small amplitudes. The envelopes for events  $>50^\circ$  are processed with a window length of 60 s, and 30 s for the rest, all with a 50% overlap.

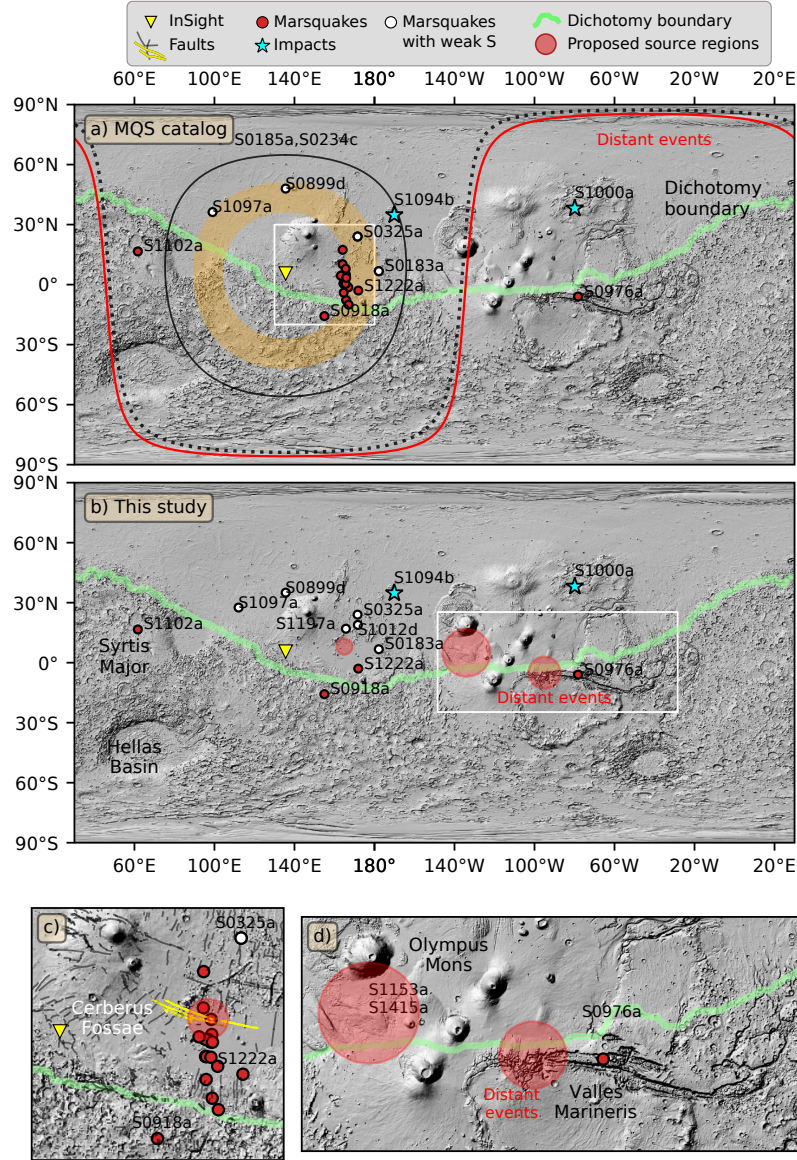


**Figure 6.** Proposed regions of seismic activity. (a) Current state from the V14 catalog (InSight Marsquake Service, 2023), including the interpretations from the visual alignments adopted since Giardini et al. (2020). The orange-colored ring around InSight denotes the distance range (32-46°) for the events with weak or no S-wave. The red curve at 90° represents the distant events class. The dotted curve indicates the distances for S1153a ( $84.8 \pm 10^\circ$ ) and S1415a ( $88.2 \pm 9.6^\circ$ ) as reported by MQS. (b) Our interpretation of the seismicity. The light red shaded circles indicate regions where there are clusters of multiple events. Symbols sizes indicate the extent of the region, not location uncertainties. Zoomed views around the Cerberus Fossae and Valles Marineris are in (c) and (d), also marked with white rectangles in (a) and (b). Fault locations in (c) around Cerberus Fossae do not reflect large uncertainties in backazimuth, allowing us to interpret that all events are associated with the fault system. The fault lines in (c) are from Knapmeyer et al. (2006) and Perrin et al. (2022), where the faults in yellow show the Cerberus Fossae system. The background map and the equatorial dichotomy boundary are from Smith et al. (2001) and Andrews-Hanna et al. (2008), respectively.

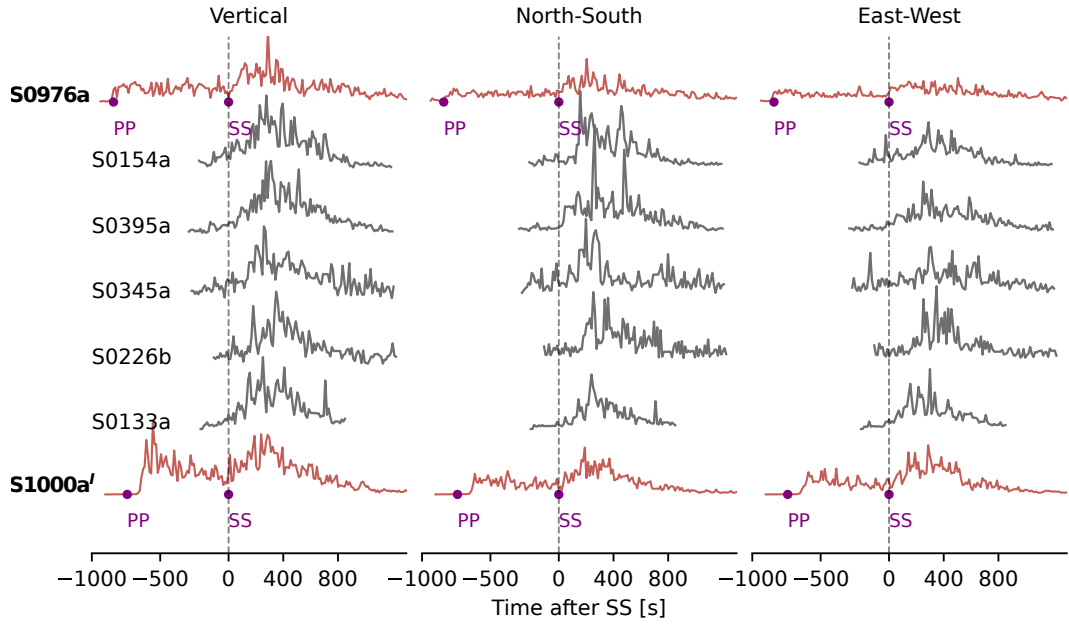


**Figure 7.** The class of most distant events, bound by the template events S0976a and S1000a<sup>T</sup> shown in red with bold font. The purple dots are the MQS phase picks used to determine distances for the templates. Time series show normalized vertical component envelopes. The template events are aligned on their SS phase picks. Other events are aligned with their energy onset which we interpret as S-waves.

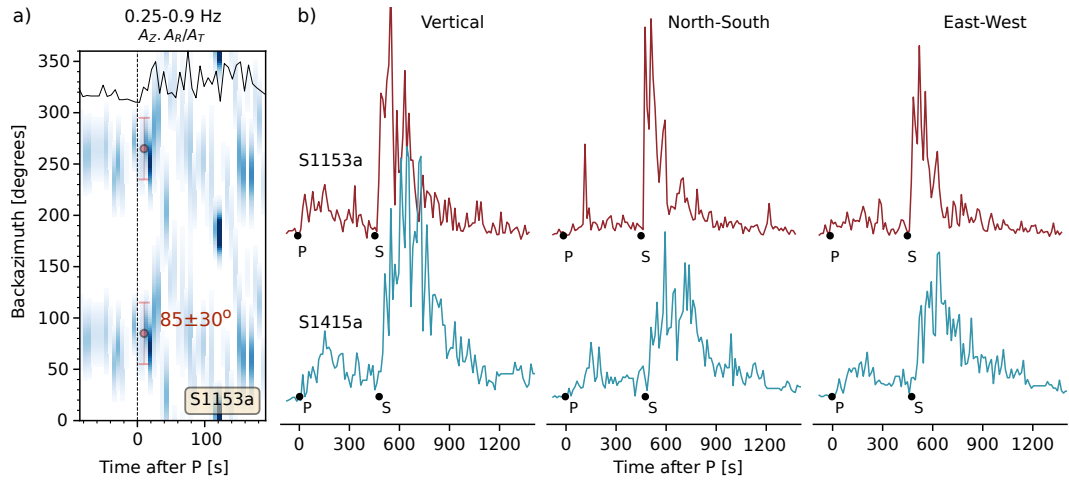


**Figure 8.** Backazimuth analysis and envelopes for the S1153a and S1415a event pair. (a) Backazimuth estimation for S1153a. (b) Three-component envelopes computed between 0.25–0.9 Hz using the VBB data in acceleration. Seismic phase picks from MQS are shown as black dots. The picking uncertainties for P and S are  $\pm 20$  and  $\pm 10$  s, respectively, for both events. See Figure S7c for the similarity warping path.

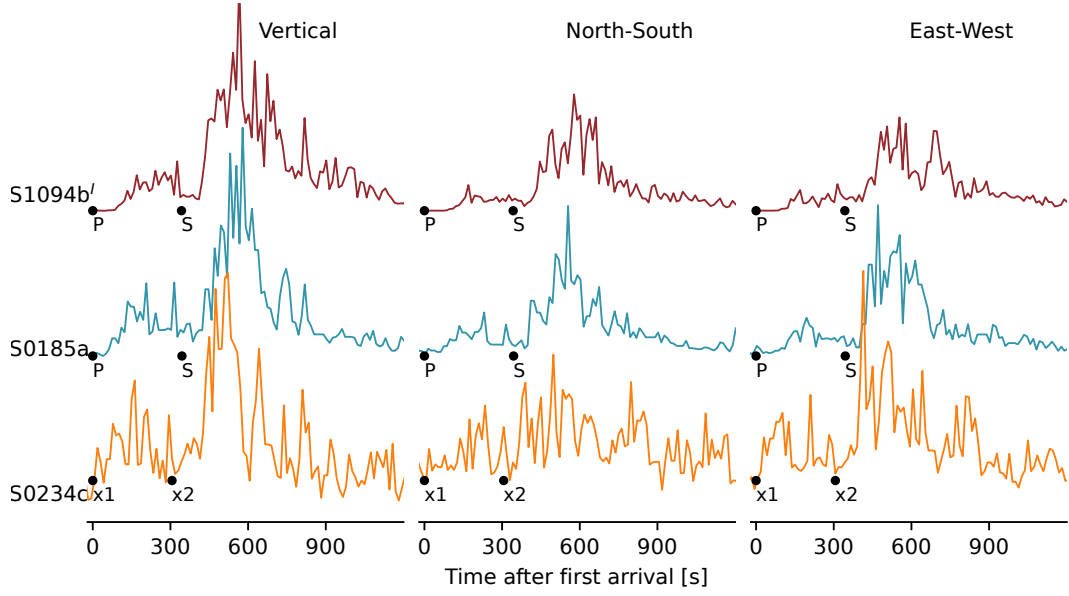


**Figure 9.** S1094b<sup>I</sup> class. The dots are the phase picks from the V14 catalog. MQS identified two phases for S0234c and labeled them as unknown (x1 and x2).

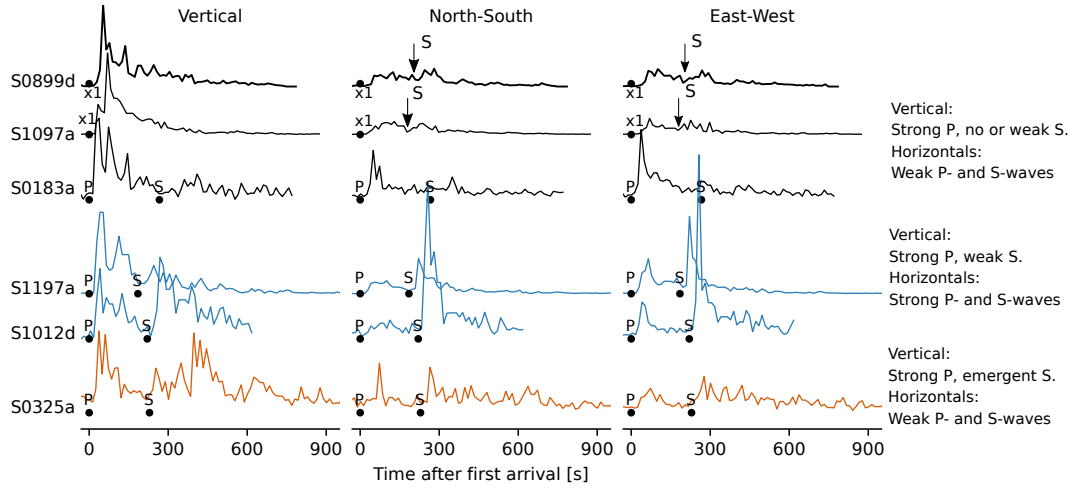


**Figure 10.** S0899d-like events with three sub-classes. MQS phase picks are denoted with dots. Only x1 picks were identified for S0899d and S1097a, though frequency-time domain polarisation analysis suggests these are P-wave energy. We propose new S-picks for both events using the horizontal components as shown with the down-pointing arrows.

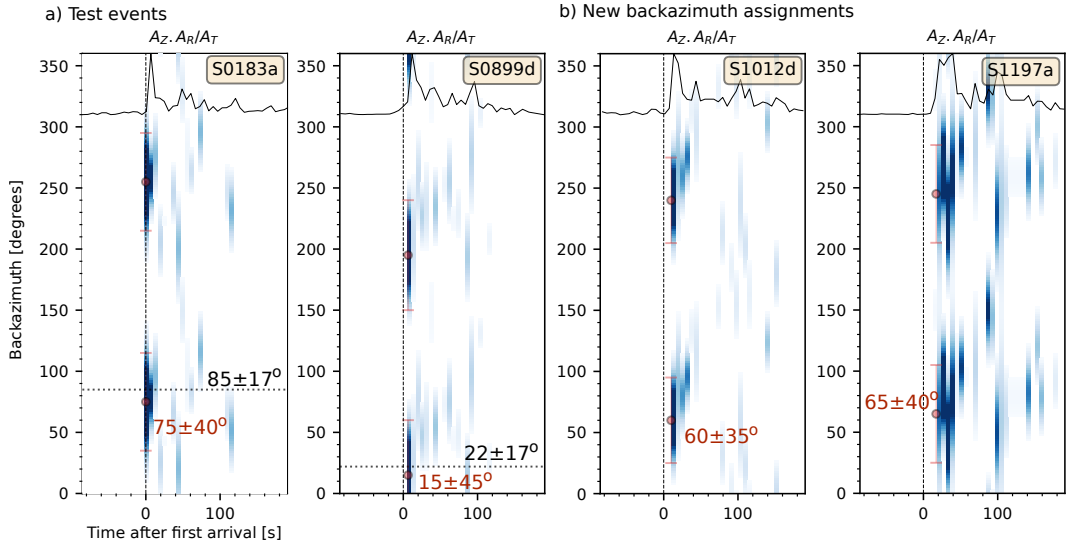


**Figure 11.** Envelope-based backazimuth estimates for S1012d and S1197a, events at similar distances to S0899d with weak or no S-waves. The dotted horizontal lines in (a) are the backazimuth values reported in the V14 catalog, while orange circles with error bars are our preferred backazimuth estimates. The similarity to the MQS values from V14 validates the grid search approach. (b) S1012d and S1197a are events without backazimuth estimates in V14. Other details follow Figure 4.

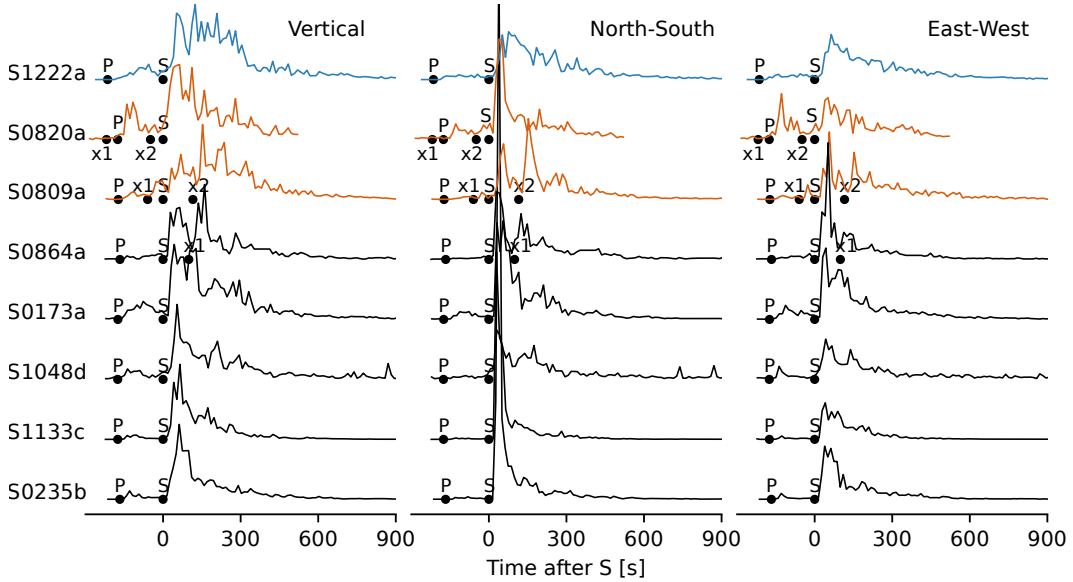


**Figure 12.** Three-component envelopes for S1222a and a subset of Cerberus Fossae events. The seismic phase picks from V14 are marked with dots. S0820a and S0809a (orange envelopes) are interpreted by MQS as double-events (Ceylan et al., 2022) with the additional phases marked as x1 and x2, instead of P and S, respectively.

## References

- Andrews-Hanna, J. C., Zuber, M. T., & Banerdt, W. B. (2008). The Borealis basin and the origin of the martian crustal dichotomy. *Nature*, *453*(7199), 1212–1215.
- Banerdt, W. B., Smrekar, S. E., Banfield, D., Giardini, D., Golombek, M., Johnson, C. L., ... Wieczorek, M. (2020). Initial results from the InSight mission on Mars. *Nat. Geosci.*, *13*(3), 183–189. doi: 10.1038/s41561-020-0544-y
- Banfield, D., Spiga, A., Newman, C., Forget, F., Lemmon, M., Lorenz, R., ... Banerdt, W. B. (2020, Mar 01). The atmosphere of mars as observed by insight. *Nature Geoscience*, *13*(3), 190–198. doi: 10.1038/s41561-020-0534-0
- Beghein, C., Li, J., Weidner, E., Maguire, R., Wookey, J., Lekić, V., ... Banerdt, W. (2022). Crustal anisotropy in the martian lowlands from surface waves. *Geophysical Research Letters*, *49*(24), e2022GL101508. doi: <https://doi.org/10.1029/2022GL101508>
- Böse, M., Clinton, J. F., Ceylan, S., Euchner, F., van Driel, M., Khan, A., ... Banerdt, W. B. (2017). A probabilistic framework for single-station location of seismicity on Earth and Mars. *Phys. Earth Planet. Inter.*, *262*, 48–65. doi: <https://doi.org/10.1016/j.pepi.2016.11.003>
- Böse, M., Giardini, D., Stähler, S., Ceylan, S., Clinton, J. F., van Driel, M., ... Banerdt, W. B. (2018). Magnitude Scales for Marsquakes. *Bull. Seismol. Soc. Am.*, *108*(5A), 2764–2777. doi: <https://doi.org/10.1785/0120180037>
- Byrne, P. K., Klimczak, C., Celâl Şengör, A. M., Solomon, S. C., Watters, T. R., & Hauck, S. A., II. (2014, Apr 01). Mercury’s global contraction much greater than earlier estimates. *Nature Geoscience*, *7*(4), 301–307. doi: 10.1038/ngeo2097
- Ceylan, S., Clinton, J. F., Giardini, D., Böse, M., Charalambous, C., van Driel, M., ... Perrin, C. (2021). Companion guide to the marsquake catalog from InSight, Sols 0–478: Data content and non-seismic events. *Phys. Earth Planet. Inter.*, *310*, 106597. doi: <https://doi.org/10.1016/j.pepi.2020.106597>
- Ceylan, S., Clinton, J. F., Giardini, D., Stähler, S. C., Horleston, A., Kawamura, T., ... Banerdt, W. B. (2022). The marsquake catalogue from InSight, sols 0–1011. *Phys. Earth Planet. Inter.*, 106943. doi: <https://doi.org/10.1016/j.pepi.2022.106943>
- Clinton, J., Ceylan, S., van Driel, M., Giardini, D., Stähler, S., Böse, M., ... Stott, A. (2021). The Marsquake catalogue from InSight, sols 0–478. *Phys. Earth Planet. Inter.*, *310*, 106595. doi: <https://doi.org/10.1016/j.pepi.2020.106595>
- Clinton, J., Giardini, D., Böse, M., Ceylan, S., van Driel, M., Euchner, F., ... Teanby, N. A. (2018). The marsquake service: Securing daily analysis of SEIS data and building the martian seismicity catalogue for InSight. *Space Sci. Rev.*, *214*(8).
- Coles, K. S., Tanaka, K. L., & Christensen, P. R. (2019). *The Atlas of Mars: Mapping its Geography and Geology*. Cambridge University Press. doi: 10.1017/9781139567428
- Daubar, I. J., Fernando, B., Garcia, R. F., & the InSight Impacts Working Group. (2023). InSight seismic events confirmed as impacts thus far. 2616, presented at the 54th Lunar and Planetary Science Conference, March 13–17, 2023.
- Durán, C., Khan, A., Ceylan, S., Charalambous, C., Kim, D., Drilleau, M., ... Giardini, D. (2022). Observation of a core-diffracted P-wave from a farside impact with implications for the lower-mantle structure of Mars. *Geophysical Research Letters*, *49*(21), e2022GL100887. doi: <https://doi.org/10.1029/2022GL100887>
- Durán, C., Khan, A., Ceylan, S., Zenhäusern, G., Stähler, S., Clinton, J., & Giardini, D. (2022). Seismology on mars: An analysis of direct, reflected, and converted seismic body waves with implications for interior structure. *Phys. Earth Planet. Inter.*, *325*, 106851. doi: <https://doi.org/10.1016/j.pepi.2022.106851>
- Garcia, R. F., Daubar, I. J., Beucler, É., Posiolova, L. V., Collins, G. S., Lognonné,

- P., ... Banerdt, W. B. (2022). Newly formed craters on Mars located using seismic and acoustic wave data from InSight. *Nat. Geosci.*, *15*(10), 774-780. doi: 10.1038/s41561-022-01014-0
- Giardini, D., Lognonné, P., Banerdt, W. B., Pike, W. T., Christensen, U., Ceylan, S., ... Yana, C. (2020). The Seismicity of Mars. *Nat. Geosci.* doi: 10.1038/s41561-020-0539-8
- Golombek, M. P., Banerdt, W. B., Tanaka, K. L., & Tralli, D. M. (1992). A prediction of Mars seismicity from surface faulting. *Science*, *258*(5084), 979-981. doi: 10.1126/science.258.5084.979
- Gudkova, T. V., Batov, A. V., & Zharkov, V. N. (2017, Nov 01). Model estimates of non-hydrostatic stresses in the Martian crust and mantle: 1—two-level model. *Solar System Research*, *51*(6), 457-478. doi: 10.1134/S003809461706003X
- Harris, C. R., Millman, K. J., van der Walt, S. J., Gommers, R., Virtanen, P., Cournapeau, D., ... Oliphant, T. E. (2020). Array programming with NumPy. *Nature*, *585*(7825), 357-362. doi: 10.1038/s41586-020-2649-2
- Horleston, A., Clinton, J., Ceylan, S., Giardini, D., Charalambous, C., Irving, J., ... Banerdt, W. (2022). The far side of Mars: two distant marsquakes detected by InSight. *The Seismic Record*. doi: 10.1785/0320220007
- InSight Mars SEIS Data Service. (2019a). *InSight SEIS Data Bundle. PDS Geosciences (GEO) Node*. doi: {10.17189/1517570}
- InSight Mars SEIS Data Service. (2019b). *SEIS raw data, InSight Mission. IPGP, JPL, CNES, ETHZ, ICL, MPS, ISAE-Supaero, LPG, MFSC*. doi: {10.18715/SEIS.INSIGHT.XB\\_2016}
- InSight Marsquake Service. (2020). *Mars Seismic Catalogue, InSight Mission; V3 2020-07-01*. ETHZ, IPGP, JPL, ICL, ISAE-Supaero, MPS, Univ. Bristol. Retrieved from <http://www.insight.ethz.ch/seismicity/catalog/v3> doi: 10.12686/a8
- InSight Marsquake Service. (2022). *Mars Seismic Catalogue, InSight Mission; V12 2022-10-01*. ETHZ, IPGP, JPL, ICL, Univ. Bristol. Retrieved from <https://www.insight.ethz.ch/seismicity/catalog/v12> doi: 10.12686/a18
- InSight Marsquake Service. (2023). *Mars Seismic Catalogue, InSight Mission; V14 2023-04-01*. ETHZ, IPGP, JPL, ICL, Univ. Bristol. Retrieved from <https://www.insight.ethz.ch/seismicity/catalog/v14> doi: 10.12686/a21
- Irving, J., Antonangeli, D., Banerdt, B., Li, J., Bozdog, E., Stähler, S., ... Stutzmann, E. (2022). First observations of seismic waves travelling through the martian core. DI44A-02, presented at 2022 AGU Fall Meeting, 12-16 December.
- Kawamura, T., Clinton, J. F., Zenhausern, G., Ceylan, S., Horleston, A. C., Dahmen, N. L., ... Banerdt, W. B. (2023). S1222a - the largest marsquake detected by InSight. *Geophysical Research Letters*, *50*(5), e2022GL101543. doi: <https://doi.org/10.1029/2022GL101543>
- Kedar, S., Panning, M. P., Smrekar, S. E., Stähler, S. C., King, S. D., Golombek, M. P., ... Banerdt, W. B. (2021). Analyzing low frequency seismic events at Cerberus Fossae as long period volcanic quakes. *Journal of Geophysical Research: Planets*, *126*(4), e2020JE006518. doi: <https://doi.org/10.1029/2020JE006518>
- Khan, A., Ceylan, S., van Driel, M., Giardini, D., Lognonné, P., Samuel, H., ... Banerdt, W. B. (2021). Upper mantle structure of Mars from InSight seismic data. *Science*, *373*(6553), 434-438. doi: 10.1126/science.abf2966
- Khan, A., Sossi, P., Liebske, C., Rivoldini, A., & Giardini, D. (2022). Geophysical and cosmochemical evidence for a volatile-rich Mars. *Earth and Planetary Science Letters*, *578*, 117330. doi: 10.1016/j.epsl.2021.117330
- Khan, A., van Driel, M., Böse, M., Giardini, D., Ceylan, S., Yan, J., ... Banerdt, W. B. (2016). Single-station and single-event marsquake location and inversion for structure using synthetic Martian waveforms. *Phys. Earth Planet. Inter.*

- 258, 28–42. doi: <https://doi.org/10.1016/j.pepi.2016.05.017>
- Kim, D., Banerdt, W., Ceylan, S., Giardini, D., Lekić, V., Lognonné, P., ... Panning, M. (2022). Surface waves and crustal structure on Mars. *Science*, 378(6618), 417–421. doi: 10.1126/science.abq7157
- Kim, D., Davis, P., Lekić, V., Maguire, R., Compaire, N., Schimmel, M., ... Banerdt, W. B. (2021). Potential pitfalls in the analysis and structural interpretation of seismic data from the Mars InSight mission. *Bull. Seismol. Soc. Am.*, 111(6), 2982–3002. doi: 10.1785/0120210123
- Kim, D., & et al. (2023). Global average crustal thickness revealed by surface waves orbiting Mars. *Geophysical Research Letters*, this issue(n/a), n/a. doi: n/a
- Kim, D., Lekic, V., Irving, J., Schmerr, N., Knapmeyer-Endrun, B., Joshi, R., ... Banerdt, W. (2021). Improving constraints on planetary interiors with PPs receiver functions. *Journal of Geophysical Research: Planets*, 126(11), e2021JE006983. doi: <https://doi.org/10.1029/2021JE006983>
- Kim, D., Stähler, S., Ceylan, S., Lekic, V., Maguire, R., Zenhäusern, G., ... Banerdt, W. B. (2023). Structure along the martian dichotomy constrained by rayleigh and love waves and their overtones. *Geophysical Research Letters*, n/a(n/a), e2022GL101666. doi: <https://doi.org/10.1029/2022GL101666>
- Knapmeyer, M., Oberst, J., Hauber, E., Wählisch, M., Deuchler, C., & Wagner, R. (2006). Working models for spatial distribution and level of mars' seismicity. *Journal of Geophysical Research: Planets*, 111(E11), E11006. doi: <https://doi.org/10.1029/2006JE002708>
- Knapmeyer, M., Stähler, S. C., Plesa, A.-C., Ceylan, S., Charalambous, C., Clinton, J., ... Banerdt, W. B. (2023). The global seismic moment rate of Mars after event S1222a. *Geophysical Research Letters*. doi: accepted
- Knapmeyer-Endrun, B., Panning, M. P., Bissig, F., Joshi, R., Khan, A., Kim, D., ... Banerdt, W. B. (2021). Thickness and structure of the martian crust from insight seismic data. *Science*, 373(6553), 438–443. doi: 10.1126/science.abf8966
- Krischer, L., Megies, T., Barsch, R., Beyreuther, M., Lecocq, T., Caudron, C., & Wassermann, J. (2015). ObsPy: a bridge for seismology into the scientific Python ecosystem. *Comput. Sci. Discov.*, 8(1), 014003.
- Li, J., Beghein, C., Wookey, J., Davis, P., Lognonné, P., Schimmel, M., ... Banerdt, W. B. (2022). Evidence for crustal seismic anisotropy at the insight lander site. *Earth and Planetary Science Letters*, 593, 117654. Retrieved from <https://www.sciencedirect.com/science/article/pii/S0012821X22002904> doi: <https://doi.org/10.1016/j.epsl.2022.117654>
- Lognonné, P., Banerdt, W., Giardini, D., Pike, W., Christensen, U., Laudet, P., ... Wookey, J. (2019). SEIS: Insight's Seismic Experiment for Internal Structure of Mars. *Space Sci. Rev.*, 215(1), 12. doi: 10.1007/s11214-018-0574-6
- Lognonné, P., Banerdt, W., Pike, W., Giardini, D., Christensen, U., Garcia, R., ... Zweifel, P. (2020). Constraints on the shallow elastic and anelastic structure of Mars from InSight seismic data. *Nat. Geosci.* doi: 10.1038/s41561-020-0536-y
- Perrin, C., Jacob, A., Lucas, A., Myhill, R., Hauber, E., Batov, A., ... Fuji, N. (2022). Geometry and segmentation of Cerberus Fossae, Mars: Implications for Marsquake properties. *Journal of Geophysical Research: Planets*, 127(1), e2021JE007118. doi: <https://doi.org/10.1029/2021JE007118>
- Posiolova, L. V., Lognonné, P., Banerdt, W. B., Clinton, J., Collins, G. S., Kawamura, T., ... Zenhäusern, G. (2022). Largest recent impact craters on Mars: Orbital imaging and surface seismic co-investigation. *Science*, 378(6618), 412–417. doi: 10.1126/science.abq7704
- Sakoe, H., & Chiba, S. (1978). Dynamic programming algorithm optimization for spoken word recognition. *IEEE Trans. Acoust.*, 26(1), 43–49. doi: 10.1109/TASSP.1978.1163055
- Scholz, J.-R., Widmer-Schmidrig, R., Davis, P., Lognonné, P., Pinot, B., Garcia,

- R. F., ... Banerdt, W. B. (2020). Detection, Analysis, and Removal of Glitches From InSight's Seismic Data From Mars. *Earth and Space Science*, 7(11), e2020EA001317. doi: <https://doi.org/10.1029/2020EA001317>
- Smith, D. E., Zuber, M. T., Frey, H. V., Garvin, J. B., Head, J. W., Muhleman, D. O., ... Sun, X. (2001). Mars Orbiter Laser Altimeter: Experiment summary after the first year of global mapping of Mars. *Journal of Geophysical Research: Planets*, 106(E10), 23689-23722. doi: <https://doi.org/10.1029/2000JE001364>
- Spohn, T., Hudson, T. L., Witte, L., Wippermann, T., Wisniewski, L., Kedziora, B., ... Grygorczuk, J. (2022, April). The InSight-HP3 mole on Mars: Lessons learned from attempts to penetrate to depth in the Martian soil. *Advances in Space Research*, 69(8), 3140–3163. doi: 10.1016/j.asr.2022.02.009
- Stähler, S. C., Khan, A., Banerdt, W. B., Lognonné, P., Giardini, D., Ceylan, S., ... Smrekar, S. E. (2021). Seismic detection of the martian core. *Science*, 373(6553), 443–448. doi: 10.1126/science.abi7730
- Stähler, S. C., Mittelholz, A., Perrin, C., Kawamura, T., Kim, D., Knapmeyer, M., ... Banerdt, W. B. (2022). Tectonics of cerberus fossae unveiled by marsquakes. *Nat. Astronomy*, 6(12), 1376-1386. doi: 10.1038/s41550-022-01803-y
- Tavenard, R., Faouzi, J., Vandewiele, G., Divo, F., Androz, G., Holtz, C., ... Woods, E. (2020). Tslern, a machine learning toolkit for time series data. *Journal of Machine Learning Research*, 21(118), 1-6. Retrieved from <http://jmlr.org/papers/v21/20-091.html>
- Virtanen, P., Gommers, R., Oliphant, T. E., Haberland, M., Reddy, T., Cournapeau, D., ... SciPy 1.0 Contributors (2020). SciPy 1.0: Fundamental Algorithms for Scientific Computing in Python. *Nature Methods*, 17, 261–272. doi: 10.1038/s41592-019-0686-2
- Weller, M. B. (2015). Basal Scarp (Olympus Mons, Mars). In H. Hargitai & Á. Kereszturi (Eds.), *Encyclopedia of Planetary Landforms* (pp. 137–141). New York, NY: Springer. doi: 10.1007/978-1-4614-3134-3\_14
- Zenhäusern, G., Stähler, S. C., Clinton, J. F., Giardini, D., Ceylan, S., & Garcia, R. F. (2022). Low-Frequency Marsquakes and Where to Find Them: Back Azimuth Determination Using a Polarization Analysis Approach. *Bull. Seismol. Soc. Am.*, 112(4), 1787-1805. doi: 10.1785/0120220019
- Zweifel, P., Mance, D., ten Pierick, J., Giardini, D., Schmelzbach, C., Haag, T., ... Banerdt, W. B. (2021, 10). Seismic High-Resolution Acquisition Electronics for the NASA InSight Mission on Mars. *Bull. Seismol. Soc. Am.*, 111(6), 2909-2923. doi: 10.1785/0120210071

# Mapping the seismicity of Mars with InSight

S. Ceylan<sup>1</sup>, D. Giardini<sup>1</sup>, J. F. Clinton<sup>2</sup>, D. Kim<sup>1</sup>, A. Khan<sup>1,3</sup>, S. C. Stähler<sup>1,4</sup>,  
G. Zenhäusern<sup>1</sup>, P. Lognonné<sup>5</sup>, W. B. Banerdt<sup>6</sup>

<sup>1</sup>Institute of Geophysics, ETH Zurich, Zurich, Switzerland

<sup>2</sup>Swiss Seismological Service, ETH Zurich, Zurich, Switzerland

<sup>3</sup>Institute of Geochemistry and Petrology, ETH Zurich, Zurich, Switzerland

<sup>4</sup>Physik-Institut, University of Zurich, Zurich, Switzerland

<sup>5</sup>Université Paris Cité, Institut de physique du globe de Paris, CNRS, Paris, France

<sup>6</sup>Jet Propulsion Laboratory, California Institute of Technology, Pasadena, CA, USA

## Key Points:

- We use a similarity analysis to classify noisier seismic events using the high quality marsquakes from InSight as templates
- We relocate marsquakes and update the seismicity map of Mars based on this analysis and new back azimuth estimates
- Our results suggest clusters of seismicity have occurred nearby to Valles Marineris and Olympus Mons

---

Corresponding author: Savas Ceylan, [savas.ceylan@erdw.ethz.ch](mailto:savas.ceylan@erdw.ethz.ch)

**Abstract**

InSight’s seismometers recorded more than 1300 events. Ninety-eight of these, named the low-frequency family, show energy predominantly below 1 Hz down to  $\sim 0.125$  Hz. The Marsquake Service identified seismic phases and computed distances for 42 of these marsquakes, 26 of which have backazimuths. Hence, the locations of the majority of low-frequency family events remain undetermined. Here, we use an envelope shape similarity approach to determine event classes and distances, and introduce an alternative method to estimate the backazimuth. In our similarity approach, we use the highest quality marsquakes with well-constrained distance estimates as templates, including the largest event S1222a, and assign distances to marsquakes with relatively high signal-to-noise ratio based on their similarities to the template events. The resulting enhanced catalog allows us to re-evaluate the seismicity of Mars. We find the Valles Marineris region to be more active than initially perceived, where only a single marsquake (S0976a) had previously been located. We relocated two marsquakes using new backazimuth estimates, which had reported distances of  $\sim 90^\circ$ , in the SW of the Tharsis region, possibly at Olympus Mons. In addition, two marsquakes with little or no S-wave energy have been located in the NE of the Elysium Bulge. Event epicenters in Cerberus Fossae follow a North-South trend due to uncertainties in location, while the fault system is in the NW-SE direction; therefore, these events are re-projected along the observed fault system.

**Plain Language Summary**

InSight’s seismometer recorded more than 1300 events since landing on the surface of Mars in November 2018 until it retired in December 2022. Most of the events InSight recorded are at high frequencies  $\geq 2.4$  Hz. The rest of the events, named the low-frequency family, produce signals that travel through the planet’s interior, allowing us to understand the interior structure when event locations can be determined using seismic arrivals. However, marsquakes are often weak and do not always exhibit clear seismic phases; therefore, they cannot be assigned distances using traditional techniques. Here, we use the well-understood, highest-quality events as templates to investigate and assign a source region to the weaker seismic signals. Seismicity on Mars occurs mostly along or north of the boundary between the southern highlands and northern lowlands. Valles Marineris is seismically more active than previous catalogs of located events imply. Further, we show evidence that two events likely originate from the Olympus Mons region.

**1 Introduction**

The Mars InSight mission (Banerdt et al., 2020) retired on December 21, 2022, after more than four years (1446 sols or Martian days) of successful operations. The mission deployed the first seismic station (SEIS) on the surface of the planet, comprising both a very broadband (VBB) and a short-period (SP) seismometer (Lognonné et al., 2019; Lognonné et al., 2020). The InSight payload also contained wind and pressure sensors for observing the Martian atmosphere (Banfield et al., 2020), which provided crucial information for discriminating seismic events from environmental noise sources; the HP<sup>3</sup> temperature probe (Spohn et al., 2022); and the robotic arm and cameras used for deploying SEIS and HP<sup>3</sup> on the ground (Banerdt et al., 2020).

Throughout the mission, the Marsquake Service (MQS; Clinton et al., 2018) cataloged more than 1300 signals of seismic origin (Table S1; InSight Marsquake Service, 2023) in the exceptionally high-quality and complete waveform dataset (Clinton et al., 2021; Ceylan et al., 2022). Ninety-eight of these events are part of the low-frequency (LF) event family showing energy predominantly below 1 Hz. The rest of the events contain energy mostly above 2.4 Hz and are classified as the high-frequency (HF) family.

For events in the LF family, when seismic phases can be identified (typically direct P and S, or their surface reflections PP and SS for distant events  $\gtrsim 100^\circ$ ), MQS determines event distances using the theoretical travel times from the model set of Stähler et al. (2021) following the single station location algorithm described in Khan et al. (2016) and Böse et al. (2017). The location of an event is obtained when a backazimuth can also be reliably determined (Böse et al., 2017), in current MQS practice, this follows the method described in Zenhäusern et al. (2022) since V12 catalog (InSight Marsquake Service, 2022).

In the V14 catalog, MQS computed distances for 42 of the 98 LF family events (Figure 1a). Twenty-four of these events are fully located with a backazimuth (hence assigned quality A), while the remaining events only have a distance estimate and are quality B or C (Table S1). The vast majority of the fully-located events cluster at distances between  $25^\circ$  and  $35^\circ$  with a backazimuth towards the East, pointing to the Cerberus Fossae region (Figure 1a).

The most distant marsquake (S0976a; Figure 1) was observed on August 25, 2021, at a distance of  $146 \pm 7^\circ$  from InSight and a backazimuth of  $101 \pm 25^\circ$ , locating the event in the Valles Marineris region (Horleston et al., 2022). Two events (S1000a and S1094b; hereinafter, referred to as S1000<sup>I</sup> and S1094b<sup>I</sup> for brevity) showed the first clear indication of seismic surface wave arrivals (Kim et al., 2022). Both of these events were later confirmed as distant impacts (Posiolova et al., 2022) with Mars-calibrated moment magnitudes (Böse et al., 2018) of  $M_W^{Ma} 4.0 \pm 0.2$  and  $4.1 \pm 0.2$  (Figure S1) and crater diameters of 130 and 150 m, respectively. Furthermore, six HF family events within 300 km of InSight have also been confirmed as impacts (Garcia et al., 2022; Daubar et al., 2023), which show dispersive acoustic signals propagating along a waveguide in the form of chirps in their coda, with strong linear polarization pointing toward the source. Finally, the largest marsquake ( $M_W^{Ma} 4.6 \pm 0.3$ ) recorded by InSight is S1222a (Kawamura et al., 2023), which occurred on May 4, 2022 (Figure S1).

Giardini et al. (2020) and Lognonné et al. (2020) give the first interpretations of the global seismicity on Mars and interior structure using limited number of both HF and LF family events recorded during the first year of the mission. Subsequently, body waves have been successfully utilized for studying the crust beneath the lander (Knapmeyer-Endrun et al., 2021; Kim, Lekic, et al., 2021; Li et al., 2022; Durán, Khan, Ceylan, Zenhäusern, et al., 2022), Martian mantle (Khan et al., 2021; Durán, Khan, Ceylan, Zenhäusern, et al., 2022; Durán, Khan, Ceylan, Charalambous, et al., 2022; Khan et al., 2022) and core (Stähler et al., 2021; Durán, Khan, Ceylan, Zenhäusern, et al., 2022; Khan et al., 2022; Irving et al., 2022). Kim et al. (2022) obtained the average crustal velocity structure along the minor-arc paths using Rayleigh waves observed in S1000a<sup>I</sup> and S1094b<sup>I</sup> (Posiolova et al., 2022). Most recently, surface wave studies of S1222a enabled us to further understand crustal anisotropy by using fundamental-mode Rayleigh and Love waves (Beghein et al., 2022) and together with their overtones (Kim et al., 2023). In the same record, Rayleigh waves that orbit around Mars have been also detected and used for estimating the planet’s average crustal thickness (Kim & et al., 2023).

The large number of noisy events is not surprising, since marsquakes are low-amplitude and the background seismic noise at InSight is highly variable. Interpreting these noisier events without any distance estimate is challenging. In order to overcome this limitation, Giardini et al. (2020) introduced an alignment-based methodology where the weak marsquakes are assigned a distance depending on their similarities with the highest-quality events whose distances were assumed fixed or anchored. In their approach, the events are visually aligned based on the predicted travel times of seismic phases using an interior reference model. Since V3 catalog (InSight Marsquake Service, 2020), MQS adopted this visual alignment approach in their locations as an alternative to interpret the events using a recent reference model from Stähler et al. (2021).

While the structural studies thus far have used the events with the highest signal-to-noise (SNR) ratio, the vast majority of the seismic events and their waveform characteristics (e.g., secondary arrivals in the signal coda and high-frequency content of some LF family events) remain to be understood. Here, we extend the visual alignment approach by introducing the Dynamic Time Warping algorithm (Sakoe & Chiba, 1978), and apply it to a larger set of LF family events now available. We first classify the relatively weaker signals using the events with the highest SNR ratio as templates. Then, we re-evaluate the seismicity on Mars in light of similarities and known tectonic regions.

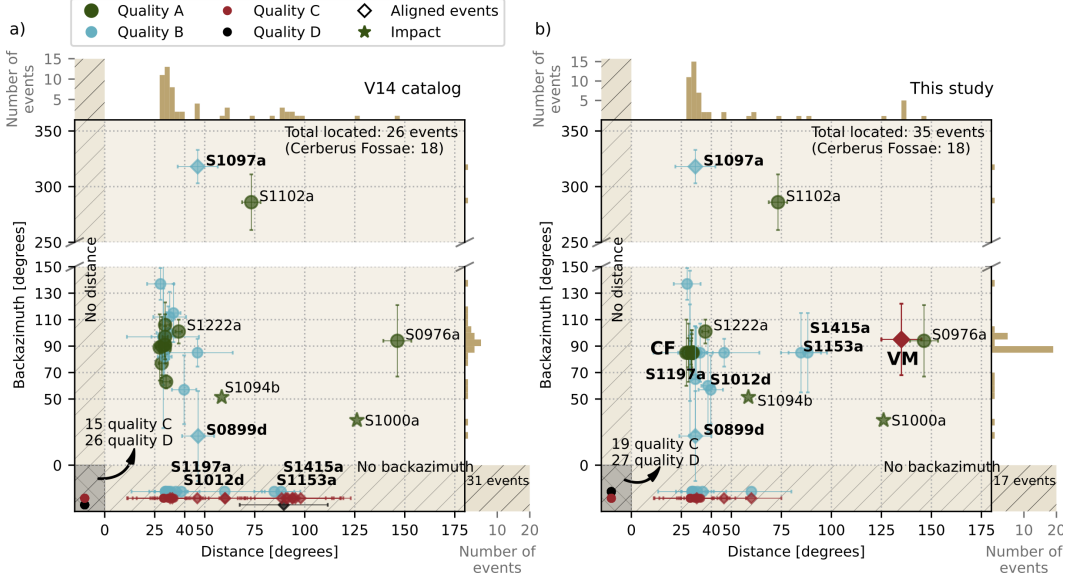


**Figure 1.** Distance and backazimuth distribution of the LF-family events in (a) the V14 catalog (InSight Marsquake Service, 2023), and (b) this study. The confirmed impacts, S1000a<sup>I</sup> and S1094b<sup>I</sup>, are denoted by stars. The 6 events labelled in bold-face have locations that are newly introduced or are modified in this study. Note a number of events without back azimuths also have their distances revised. Diamonds indicate events in V14 where the distance is only provided by visual alignments. The colors and marker sizes show the event qualities as indicated in Table S1. The histograms indicate the number of events for distance (top) and backazimuth (right). A majority of the catalog includes events at distances around 30° and a backazimuth towards East (80–100°), pointing to the Cerberus Fossae region. The hatched regions show events without backazimuth or distance estimates. The errors bars show the uncertainties in distance and backazimuth. See Figure S1 for the distance and  $M_W^{Ma}$  distributions, and Table S2 for a summary of re-evaluated events and our modifications. CF: Cerberus Fossae, VM: Valles Marineris.

## 2 Data and methods

For our analysis, we use spectral envelopes derived from the 20 samples-per-second (sps) VBB waveform data from the LF family events cataloged during the entire mission. All the events and waveforms (InSight Mars SEIS Data Service, 2019b, 2019a) are publicly available with the release of the V14 catalog (InSight Marsquake Service, 2023). A breakdown of the catalog, including the HF events, is provided in Table S1.

Our method builds on the visual alignment approach of Giardini et al. (2020). In the visual alignments, event envelopes of both low SNR events and high quality are com-

pared, and weaker events are assigned a relative distance using the envelope similarities, theoretical travel time curves and the events with pick-based distances as anchors. However, the low SNR events are often found to be similar to multiple template events, i.e., in the shape and length of their S-wave coda. Consequently, interpretation of events is often challenging and ambiguous.

In order to address these particular cases, we introduce the dynamic time warping (DTW; Sakoe & Chiba, 1978) algorithm to measure event similarity using the shape of their spectral envelopes (Figures 2 and 3). Additionally, we use an alternative approach to determine new backazimuths for a subset of events using a grid search for the waveform envelopes, as illustrated in Figure 4. Finally, we provide distances for the events with lower SNR by finding the best matches to the collection of high-quality template events, with addition insights from backazimuths in some cases, and separate the seismicity into classes (Figure 5). Our analysis assumes the source and structural effects along the propagation path, such as attenuation and scattering, are negligible.

## 2.1 Similarity analysis

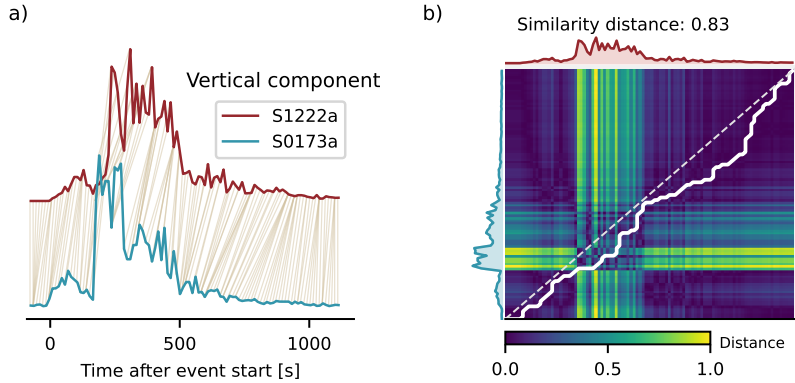


**Figure 2.** Example of the DTW method (Sakoe & Chiba, 1978) to determine the shape similarity between the spectral envelopes of two of the high-quality marsquakes, S1222a and S0173a. (a) The final optimal point-wise pairings between the event envelopes. The light-brown lines indicate matching data points with minimum distance in  $\|L_1\|$  norm. (b) The warping path and cross-similarity matrix. The color bar shows the normalized distance measure for similarity, with larger values indicating less similarity. The warping path would be perfectly diagonal (dashed line) if the envelopes were identical. The deviation from the ideal path for these two events is reasonably close to the diagonal.

The data processing workflow we use to generate envelopes is summarized in Figure S2. First, we remove the instrument response to obtain acceleration time series and rotate the VBB data into the ZNE (vertical-North-East) coordinate frame. Then, we compute spectrograms for all three components using a window length of 30 s and an overlap of 60%. Finally, we obtain the envelopes by summing the spectral amplitudes in power for each component in linear scale along the frequency axis between 0.25 and 0.9 Hz, which is a frequency window that is rich in energy for the majority of LF family events (Ceylan et al., 2022). The upper bound is intentionally below 1 Hz to avoid an artifact caused by the electronics (Zweifel et al., 2021). The envelopes have a sample point every 12 seconds. Although different parameters in terms of physical units, window lengths and overlaps can be used, the selected parameters are preferred through experience gathered throughout the mission so as to allow for comparison of events from different distances. We use

the vertical component for measuring envelope similarities since it is the least-contaminated by atmospheric disturbances.

For data regularization in advance of the DTW (Figures 2 and 3), a short time-window around significant glitches in the time series are masked in the spectral envelopes. Glitches are ubiquitous artifacts observed in the data (Scholz et al., 2020; Ceylan et al., 2021) and may lead to inaccurate interpretations (Kim, Davis, et al., 2021). For masking, we replace the original envelope values with the mean of adjacent data points. The glitch windows have been manually identified by the MQS. The spectral envelopes start 90 s prior to the energy onset as marked in the V14 catalog. The end times are manually assigned for the few events that have a very long duration ( $>1\text{h}$ ); otherwise, we use the signal end from the catalog (InSight Marsquake Service, 2023). For similarity metrics, the point-wise distances in Figure 2a are computed using the  $\|L_1\|$  norm because of its stability and relative insensitivity to noisy time series. The final similarity values (Figure S3) are normalized with the warping path length to account for differences in the duration of the time series.

The DTW method is not suitable to use in an automated style for our purposes. For instance, an event with no apparent S-wave energy may show a relatively higher degree of similarity to another event with strong S-wave (e.g., S1097a and S0235b in Figure 3a and b). Therefore, an a-priori knowledge of events for their available phase picks, polarization attributes and P- and S-wave coda lengths are required for interpretation.

## 2.2 Backazimuth estimation

Backazimuth is defined as the angle between the seismic station and epicenter with respect to North in a station-centric coordinate frame. MQS initially determined backazimuth from the 3-component particle motions in the time domain (Böse et al., 2017), though recently migrated to a more rigorous approach using polarization measured using both P and S-wave arrivals in the frequency-time domain (Zenhäusern et al., 2022). MQS does not assign backazimuths when the results from either method are interpreted to be unstable.

In an attempt to increase the number of events with assigned backazimuths, we adopt a grid search method using the envelope timeseries. A variation of this approach has been successfully applied to determine the backazimuth of the HF events in Stähler et al. (2022). Here, using well documented events, we demonstrate that our approach can recover similar backazimuths to other methods. Figures 4 and S4–S6 show how this approach performs for the 2 distant impacts as well as the large events S0235b and S1222a.

In order to find the most plausible rotation angle range, we rotate the spectral envelopes for  $360^\circ$  with an increment of  $2^\circ$ . Ideally, in the presence of P-waves, the energy ratio of vertical (Z) and radial (R) components compared to the transverse (T) must be maximized when the rotation is in the same direction as the true backazimuth. As a reliability check, the transverse-to-radial ratio should have maxima at  $90^\circ$  perpendicular to the vertical-to-transverse component ratio. In our test cases, the cross-power of Z and R components ( $Z.R/T$ ) better accentuates the results (Figure 4c, S4-S6), which makes picking backazimuths easier. We choose the backazimuth values using the first concentrated amplitude ratios in the time window directly after the initial phase arrivals and assign the uncertainties visually. Since we only use envelope amplitudes, we cannot eliminate the  $180^\circ$  ambiguity (Figure 4).

## 3 Results and discussion

The InSight seismicity catalog (Clinton et al., 2021; Ceylan et al., 2022) is a collective inventory of work from the InSight science team that includes not only the lo-

cations provided by MQS, but also locations of known impacts (Posiolova et al., 2022; Garcia et al., 2022), alternative source interpretations (Kedar et al., 2021), seismic phase picks (e.g. Khan et al., 2021; Stähler et al., 2021; Durán, Khan, Ceylan, Zenhäusern, et al., 2022), and distance and seismic phase assignments from the visual alignments (Giardini et al., 2020). Our analysis below provides new, updated alignments that allows us to assign distances to substantially more of the LF family of events, coral events into classes or group, enabling us to re-evaluate our understanding of Martian seismicity. A summary of the work is shown in Figure 5, where the various event groups are present in terms of their distance from the InSight lander. These results can be expected to included in final, post-mission catalog releases from MQS.

The map of the seismicity of Mars as contained in the MQS V14 catalog (InSight Marsquake Service, 2023) is summarized in Figure 6a, while our interpretation resulting from this analysis is in Figure 6b (also see Figures S10–S12 for each class discussed below). The seismicity on Mars appears to occur along or to the North of the dichotomy boundary. Furthermore, it is notable that 2 of the 3 template events from distances  $>90^\circ$  are the S1000a<sup>I</sup> and S1094b<sup>I</sup> impacts.

### 3.1 Distant events cluster

The so-called distant events (Figure 7) are a class of seismic signals that are bound between the 2 most distant template events, S1000<sup>I</sup> and S0976a. The low SNR signals that match this group lack any indication of P-energy and exhibit relatively long energy packages, which we interpret as S-wave coda. The visual alignments placed these events at distances  $>90^\circ$  using the length of the S-wave coda as a proxy for distance (Figures 6a and S11). The two distant template events, the only ones to lie beyond the core shadow, did not occur until late in the mission over 2.5 years after landing. Therefore, although the weak events now assigned at this distance occurred early on the mission, there was no possibility to constrain their event distances until recently.

MQS locates S0976a in the Valles Marineris region (Horleston et al., 2022),  $146\pm 7^\circ$  away from InSight. S1000a<sup>I</sup> occurred in Tempe Terra at a distance of  $126^\circ$  (Figure 6a) (Posiolova et al., 2022). In this context, we note that an independent joint seismic event-location and structure-inversion scheme predicts a location for S1000a<sup>I</sup> in excellent agreement with the imaged location (Durán, Khan, Ceylan, Zenhäusern, et al., 2022). The length of the S-wave coda for distant events is more comparable to S1000a<sup>I</sup> as it is shorter than S0976a (Figures 5 and 7), suggesting that these events occurred at a distance range of  $\sim 130\text{--}140^\circ$ , possibly closer to S1000a<sup>I</sup>.

Considering the lack of any energy that we interpret to be P-wave, as well as the emergent nature of the S-energy, the envelope-based back azimuth approach was not used to try further constrain locations for these events. The only evidence of tectonic-related seismic activity at these distances is from Valles Marineris. Valles Marineris is one of the largest canyons in the whole Solar system (Coles et al., 2019) and has been proposed as one of the most plausible candidates to produce marsquakes, using both surface faulting observations (Golombek et al., 1992) and joint inversion of gravity and topography data (Gudkova et al., 2017). It is reasonable to assume that the region is more active than might be suggested on account of the observation of a single event. Therefore, we assign these events a distance of  $130\text{--}140^\circ$ , and suggest that the source region could be in the western part of Valles Marineris (Figure 6b and d).

### 3.2 Assigning locations to S1153a and S1415a

In V14 catalog, MQS provides only distance estimates for S1153a and S1415a at  $84.8\pm 10^\circ$  and  $88.2\pm 9.6^\circ$ , respectively. In addition to being the only events in the catalog with phase-based distances at this distance, the frequency content of the events are

also remarkably similar (Figure S8). Furthermore, they show a high degree of similarity in all three components (Figures 8a and S7), suggesting that most likely both events originated from the same region.

MQS does not assign a backazimuth to either of these events due to their emergent P-arrivals and contaminated waveform characteristics (Figure S8). Applying the envelope-based grid search approach for S1153a, we obtain a backazimuth estimate of  $85\pm 30^\circ$  with the  $180^\circ$  ambiguity (Figure 8a), which places the event in a region SW of Olympus Mons. A reliable backazimuth pick was not possible for S1415a, although the P-wave energy partitioning between the horizontal components imply a value similar to S1153a in a more NE-SW direction (Figure 8b). Considering the large uncertainties for S1153a, we assume both events occurred roughly in the same region and locate them SW of Olympus Mons (Figure 6b and S10).

It is noted that in the V14 catalog and seen in Figure 1a, there is a cluster of aligned events assigned also to this distance. As described in the previous subsection, all these aligned events have been moved further away from InSight to Valles Marineris.

### 3.3 Events near to S1094b<sup>I</sup>: S0185a and S0234c

The S1094b<sup>I</sup> impact crater was detected in Amazonis Planitia at a distance of  $58.5^\circ$  with a backazimuth of  $51.4^\circ$ . Two relatively weak events S0185a and S0234c are shown to have strong similarity, as demonstrated in Figures 9 and S7b. The distance for S0185a is calculated by MQS as  $60\pm 20^\circ$ . S0234c is assigned a distance of around  $70^\circ$  through visual alignment. Neither of the events have MQS assigned backazimuths. Our similarity metrics confirm that S1094b<sup>I</sup> is very similar to S0185a, and similar to S0234c (Figure S7). Therefore, we do not modify the previously reported distances.

No reliable backazimuth for either S0185a and S0234c can be obtained from our envelope-based grid search approach. The closest seismic event with a location is S1102a ( $73.3\pm 5^\circ$ ), located in Syrtis Major Planum (Figure 6), though this event is  $20^\circ$  further out. The MQS distances for S0185a and S0234c coincide well with the eastern portion of Syrtis Major Planum; however, it is difficult to assign a specific source region without any indication of backazimuth for either of the events.

### 3.4 Events similar to S0899d: marsquakes with weak or no S-waves

S0899d has a strong arrival that can clearly be associated to a P-wave via its vertical polarization which indicates that the event comes from a direction to the North of InSight with a backazimuth of  $22\pm 30^\circ$  (Table 1, Figure 6). A subset of weak marsquakes, like S0899d, also show little-to-no S-wave energy (Figure 10) in the vertical component or have an S-to-P ratio  $\sim 1$ . The template for this class of events is S0899d, which does not have a pick-based location, although visual alignments suggest a distance of  $\sim 46^\circ$  due to its similarity to S0183a.

Here, using the envelopes, we identify for the first time S-wave arrivals for S0899d and S1097a on the horizontal components (Figure 10), and modify their aligned distances from  $46^\circ$  to  $32^\circ$  by aligning the event against the theoretical travel times from the reference model (Figures 5 and 6). S0183a remains an outlier: although the event clusters with S0899d in terms of envelope characteristics, its epicenter in the V14 catalog is at a distance of  $46^\circ$  (Figure 6). Khan et al. (2021) provides an alternative distance range and locates S0183a at  $54\text{--}59^\circ$  using differential arrival times of seismic phases from multiple events and the current knowledge of mineralogy.

S1012d and S1197a were not assigned a backazimuth in V14. Using the envelope grid search method, we propose that the events have backazimuths of  $60\pm 35^\circ$  and  $65\pm 40^\circ$ , respectively (Figure 11). This means the events locate close to S0325a, so there is now

a cluster of three events in this class (Figures 6 and S11). Due to the  $180^\circ$  ambiguity, it is possible that these events are on the opposite side of the azimuth semicircle. However, the observed seismicity on Mars appears to occur along or North of the equatorial dichotomy (Figure 6); therefore, we find our preferred backazimuth more plausible.

The tectonic source behind this event class has yet to be discovered. Giardini et al. (2020) and Khan et al. (2021) explain the lack of S-waves with distance and suggest that S-waves are attenuated between  $\sim 40$ - $60^\circ$  where seismic waves propagate through a low-velocity layer in the mantle. With more data available, the epicenters determined by MQS and our re-locations imply a scattered and closer distribution of these events; hence, distance alone cannot explain the lack of S-waves. We cannot assign a single region for these events; therefore, we attribute the decrease in S-wave energy to geometrical spreading due to strong 3D mantle structure or an S-wave low velocity layer in the lithosphere (Giardini et al., 2020; Khan et al., 2021), or source mechanism.

**Table 1.** Location parameters of S0899d class. The V14 distances with asterisks are assigned using the visual alignment rather than phase picks. We modified the previously assigned distances for S0899d and S1097a using new S-picks on Figure 7, and calculated new backazimuths for S1197a and S1012d (Figure 11). BAZ: backazimuth.

Event name	V14 Distance ( $^\circ$ )	V14 BAZ ( $^\circ$ )	This study Distance ( $^\circ$ )	This study BAZ ( $^\circ$ )
S0183a	$46.0 \pm 17.0$	$85 \pm 17$	–	–
S0899d	$46.7 \pm 10^*$	$22 \pm 30$	$32 \pm 10$	–
S1197a	$32.0 \pm 1.5$	–	–	$65 \pm 40$
S1097a	$46.2 \pm 10^*$	$318 \pm 20$	$32 \pm 10$	–
S1012d	$38.2 \pm 3.3$	–	–	$60 \pm 35$
S0325a	$39.7 \pm 6.1$	$57 \pm 20$	–	–

### 3.5 S1222a and the Cerberus Fossae class

S1222a, which occurred on May 4, 2022, is the largest event ( $M_W^{Ma} 4.6 \pm 0.2$ ) recorded since landing. The event is  $37^\circ \pm 1.6$  away from InSight, and unlike most of the LF family, shows clear Rayleigh and Love waves including their overtones. The MQS backazimuth estimate for S1222a is  $101 \pm 8^\circ$  (Kawamura et al., 2023), while using the envelope-based approach we obtain  $125^\circ \pm 15$  which is also consistent with the direction of propagation from the minor-arc surface waves (Kim et al., 2023). This suggests that the event perhaps originated closer to the Martian dichotomy boundary (Andrews-Hanna et al., 2008) than the location reported in V14 catalog. Interestingly, although the event did not originate in the Cerberus Fossae, we observe that the S1222a envelopes are largely similar to those of the LF events with excess energy in the S-wave coda from Cerberus Fossae (Figure 2 and 12).

InSight did not record any tectonic events closer than  $25^\circ$  from the station (Figure 1a). A large number of the LF-family events, which show relatively clear P- and S-wave arrivals, are located in the Cerberus Fossae region,  $25$ – $35^\circ$  away from the station due East (Durán, Khan, Ceylan, Zenhäusern, et al., 2022; Stähler et al., 2022). Within this cluster of events, the decay of P- and S-wave coda is similar, although some events show excess energy in their coda (e.g. S0173a vs S0235b; Figure S9). No new events were added to this cluster class through our study.

Stähler et al. (2022) attributes the seismicity in the Cerberus region to the active deformation caused by recent volcanism. The authors also show that the HF events come

from a similar direction as the LF family events located in the region and propose that all HF events originate from the central part of Cerberus Fossae in the form of very shallow events associated with large active volcanic dykes.

The strike of the Cerberus Fossae fault system is directed NW-SE (yellow lines in Figures 6c and S13), while the epicenters of Cerberus events follow an N-S trend. In order to be consistent with the surface observations (Knapmeyer et al., 2006; Perrin et al., 2022), we project all Cerberus events to the center of the fault system while maintaining their reported distances.

## 4 Conclusions

Contrary to pre-mission expectation (Knapmeyer et al., 2006), we find that over the lifetime of the mission, InSight did not observe a wide distribution of seismicity across the planet. Except for S1222a, seismicity was not observed on wrinkle ridges. Instead, the seismicity appears to focus on isolated tectonic features in a few distance ranges and locations along or North of the Martian dichotomy (Figure 6), implying that contraction due to cooling is not the dominant driver of present-day Martian tectonics, as proposed for other smaller terrestrial planets, Mercury and the Moon (Byrne et al., 2014):

- (i) A number of low SNR events that due to their very long duration are likely distant events and were originally located by visual alignments at distances  $>90^\circ$ , are found to be highly similar to the impact event S1000a<sup>I</sup> at  $126^\circ$  away from InSight. In light of the only evidence of a tectonic region at these distances from S0976a, these events are likely to occur in southern Tharsis region, plausibly in western Valles Marineris (Figure 6b and d). The absence of observed seismicity from the heavily faulted Tharsis region had been puzzling beforehand, but can now be explained by the fact that SS and PP waves from these distances are generally highly scattered and can only be identified as such by comparison to template events such as the S1000a<sup>I</sup>.
- (ii) Two events (S1153a and S1415a) have similar envelope shape (Figure 8b) and spectral content (Figure S2). These events have distances around  $90^\circ$  as computed by MQS. We find a backazimuth of  $85^\circ$  for S1153a (Figure 8a), and locate both of these events in the approximate area of Olympus Mons (Figure 6), which is surrounded by a basal scarp of 2–10 km height and thrust faults as young as  $<40$ Ma (Weller, 2015).
- (iii) S0185a and S0234c can be paired with the impact S1094b<sup>I</sup>. The event distances are compatible with a source region at a distance of  $\sim 60^\circ$  (Figure 5 and 9); however, since S0185a and S0234c have no convincing indication of backazimuth, we are not able to identify a single source region.
- (iv) A subset of events (S0899d class) show little or no S-wave energy, specifically on the vertical component (Figure 5). We computed backazimuths for two of the events in this class (S1012d, S1197a; Figure 11). This class of events shows no spatial clustering; therefore, the source region is unknown. The lack of stronger S-waves remains puzzling. Possible reasons are source mechanism, geometrical spreading due to strong 3D mantle structure or a relatively thin S-wave low velocity zone due to a velocity inversion in the lithosphere (Khan et al., 2021).
- (v) The main seismogenic region on InSight’s hemisphere of Mars (Figure 1) remains to be the central part of Cerberus Fossae (InSight Marsquake Service, 2023; Stähler et al., 2022), with original MQS epicenters aligned in a N-S trend (Figure 6a and c). Since the faults in the region have a strike along NW-SE direction (Perrin et al., 2022), we re-assign those events to the center of the Cerberus Fault system.

Our re-locations have no effect on the recent interior models (e.g. Khan et al., 2021; Stähler et al., 2021; Kim et al., 2022) since we do not adjust the locations or seismic phase

picks for the high-quality events. However, our re-evaluations of e.g., the distant event class, are potentially important for future studies aiming at the deep interior of Mars (e.g. Irving et al., 2022), as well as regional seismicity and global stress field estimates of the planet (e.g. Knapmeyer et al., 2023).

## 5 Open Research

The waveform data and seismicity catalog are available from InSight Mars SEIS Data Service (2019a) and InSight Mars SEIS Data Service (2019b). The InSight seismicity catalog is from InSight Marsquake Service (2023). We used the ObsPy (Krischer et al., 2015), NumPy (Harris et al., 2020) and scipy (Virtanen et al., 2020) packages for data processing. We benefited from the tslearn package of Tavenard et al. (2020) for similarity analysis.

## Acknowledgments

We acknowledge NASA, CNES, partner agencies and institutions (UKSA, SSO, DLR, JPL, IPGP-CNRS, ETHZ, ICL, MPS-MPG), and the operators of JPL, SISMOC, MSDS, IRISDMC and PDS for providing the SEIS data. Marsquake Service (MQS) operations at ETH are supported by ETH Research grant ETH-06 17-02. The authors recognise support from the ETH+ funding scheme (ETH+02 19-1: “Planet Mars”). This is InSight Contribution Number 195.

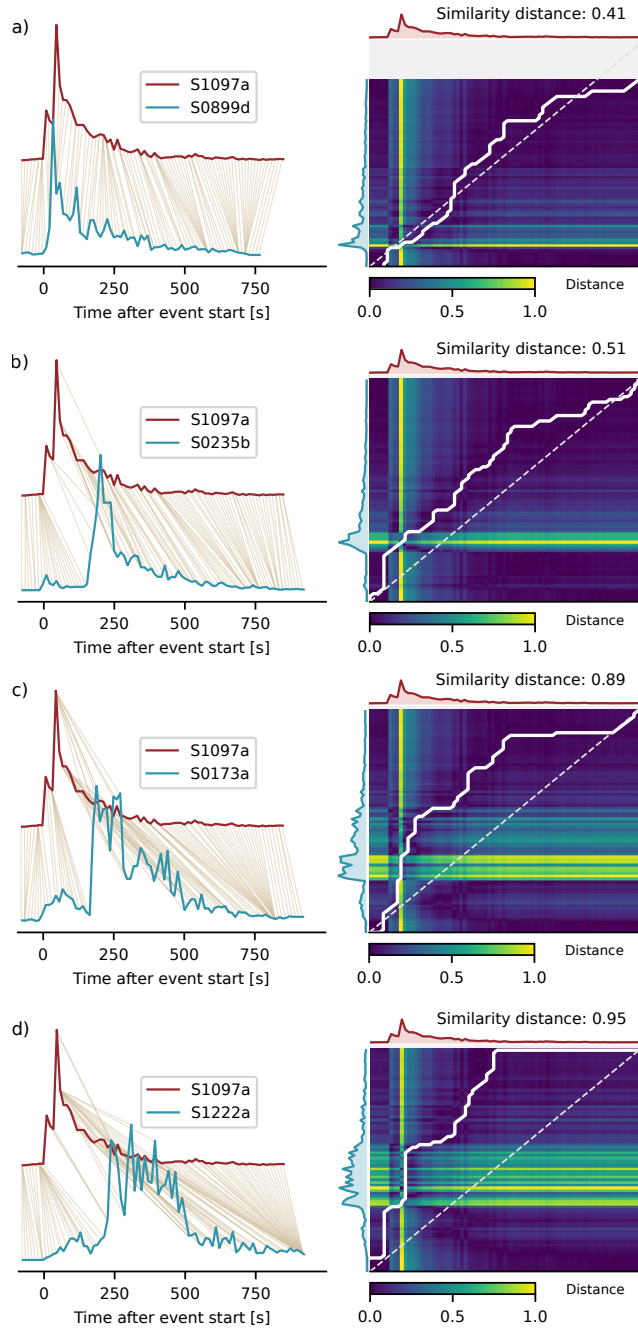


**Figure 3.** Similarity analysis for S1097a, an LF QB event without an assigned distance in the V14 catalog, against 4 template events. The final similarity distances in  $\|L_1\|$  norm are indicated in the warping path panels, where smaller values indicate higher level of similarity (Figure S3). The event is most similar to S0899d (a), another LF QB event without a pick-based distance in the catalog. Therefore, S1097a clusters within the same class. Note that the envelope shape is also significantly similar to S-wave coda of S0235b (b). The degree of similarity decreases for other templates in (c) and (d).

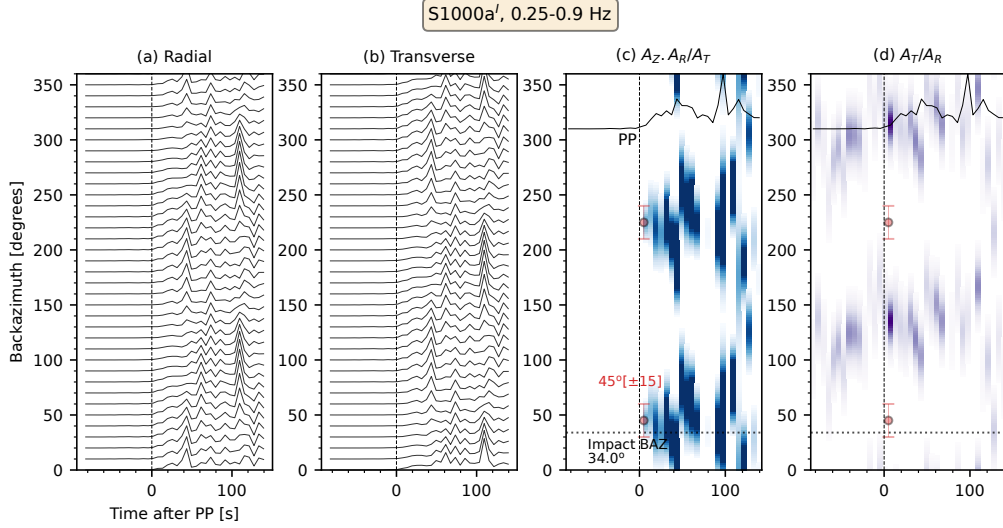


**Figure 4.** Validation of envelope-based grid search approach for backazimuth estimation using  $S1000a^I$ . The impact crater (Posiolova et al., 2022) is detected  $126.09^\circ$  away from InSight and at a backazimuth of  $34^\circ$  (Posiolova et al., 2022). The vertical dotted lines at zero time on each panel indicate the PP phase arrival time. (a) and (b) show the rotated horizontal envelopes, computed for frequencies between 0.25 and 0.9 Hz. The envelope amplitudes are normalized using the maximum of the vertical component for visualization purposes. (c) and (d) denote combined vertical (Z) and radial (R) to transverse (T) and T/R ratio, respectively. The orange circles and error bars show the preferred backazimuth pick with the ambiguity, computed using envelope amplitudes prior to normalization. For reference, the Z-component envelopes are plotted at the top of (c) and (d). The horizontal dotted lines in (c) and (d) show the true backazimuth. The color scale in (c) is saturated to make the amplitudes after the PP more visible.

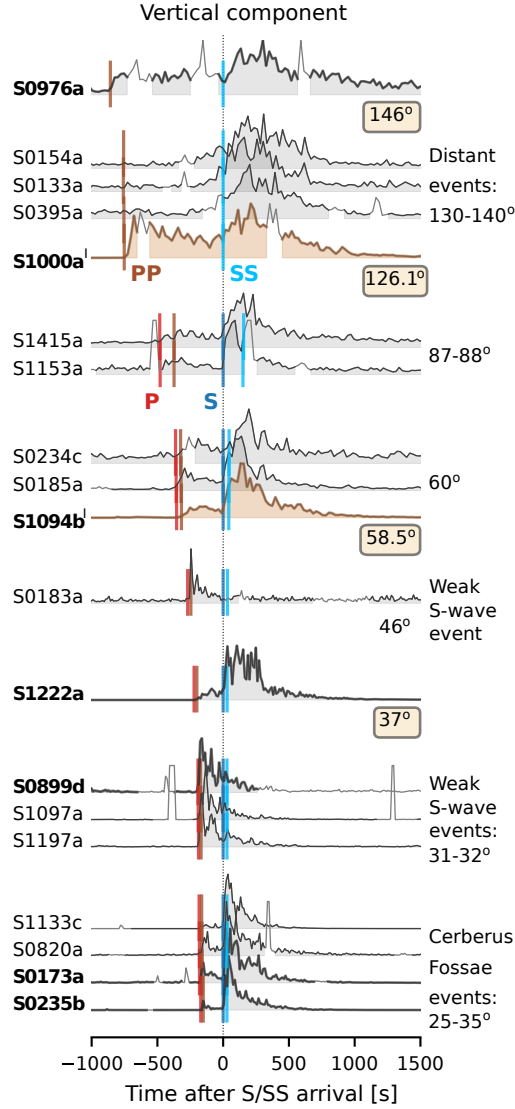


**Figure 5.** Overview of event classes. Each class is indicated by the label on the right. Template events are indicated by bold lines and font. Timeseries show the envelopes computed from vertical component acceleration data for frequencies 0.25–0.9 Hz. The light-gray parts of the envelopes show the unglitched data, note the glitches are masked for similarity processing. The 2 envelopes in a tan color are the known impacts. The distances from V14 are indicated on the right side for all template events outside of the Cerberus Fossae cluster. The zero time is the first arriving theoretical S-wave (S or SS depending on the distance) from a reference model (Stähler et al., 2021; Ceylan et al., 2022). Theoretical arrival times for P, S, PP and SS phases are marked and labelled. S0899d, S1097a and S1197a belong to the same class with S0183a, but clearly lie closer to InSight at around  $32^\circ$ . Envelopes are in log-scale to emphasize similarities at small amplitudes. The envelopes for events  $>50^\circ$  are processed with a window length of 60 s, and 30 s for the rest, all with a 50% overlap.

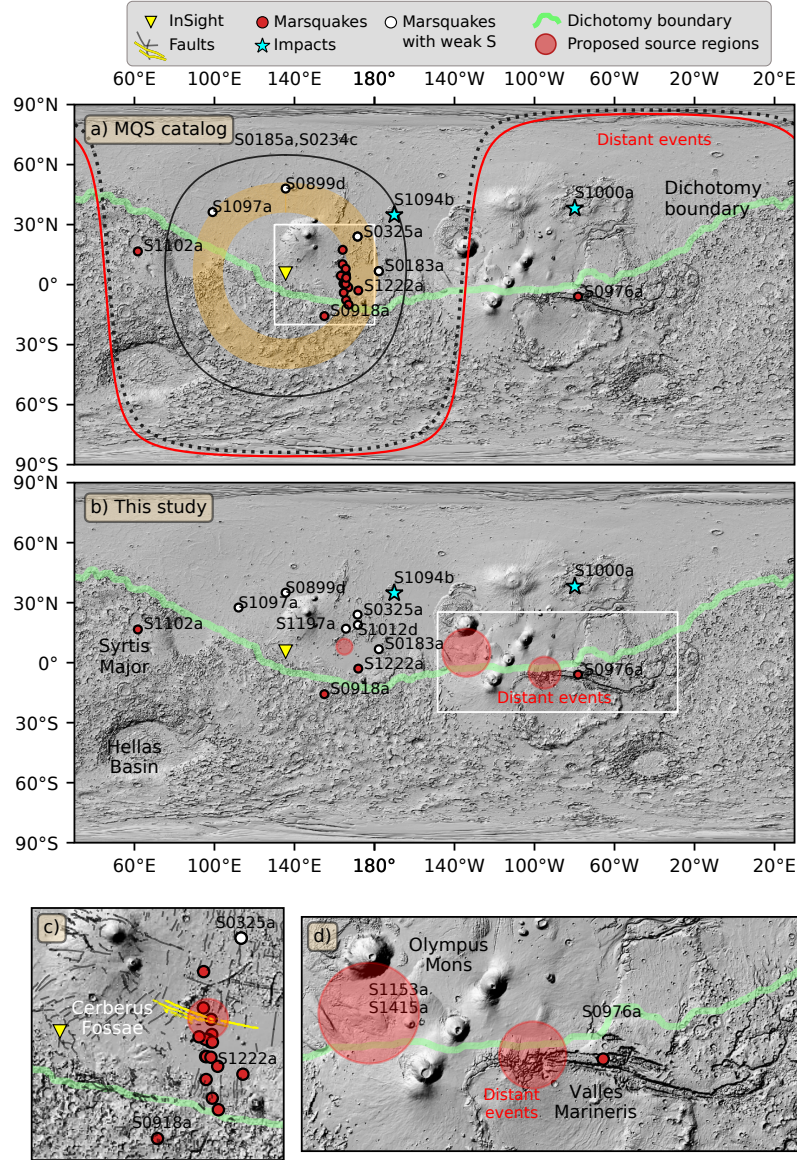


**Figure 6.** Proposed regions of seismic activity. (a) Current state from the V14 catalog (InSight Marsquake Service, 2023), including the interpretations from the visual alignments adopted since Giardini et al. (2020). The orange-colored ring around InSight denotes the distance range ( $32\text{--}46^\circ$ ) for the events with weak or no S-wave. The red curve at  $90^\circ$  represents the distant events class. The dotted curve indicates the distances for S1153a ( $84.8 \pm 10^\circ$ ) and S1415a ( $88.2 \pm 9.6^\circ$ ) as reported by MQS. (b) Our interpretation of the seismicity. The light red shaded circles indicate regions where there are clusters of multiple events. Symbols sizes indicate the extent of the region, not location uncertainties. Zoomed views around the Cerberus Fossae and Valles Marineris are in (c) and (d), also marked with white rectangles in (a) and (b). Fault locations in (c) around Cerberus Fossae do not reflect large uncertainties in backazimuth, allowing us to interpret that all events are associated with the fault system. The fault lines in (c) are from Knapmeyer et al. (2006) and Perrin et al. (2022), where the faults in yellow show the Cerberus Fossae system. The background map and the equatorial dichotomy boundary are from Smith et al. (2001) and Andrews-Hanna et al. (2008), respectively.

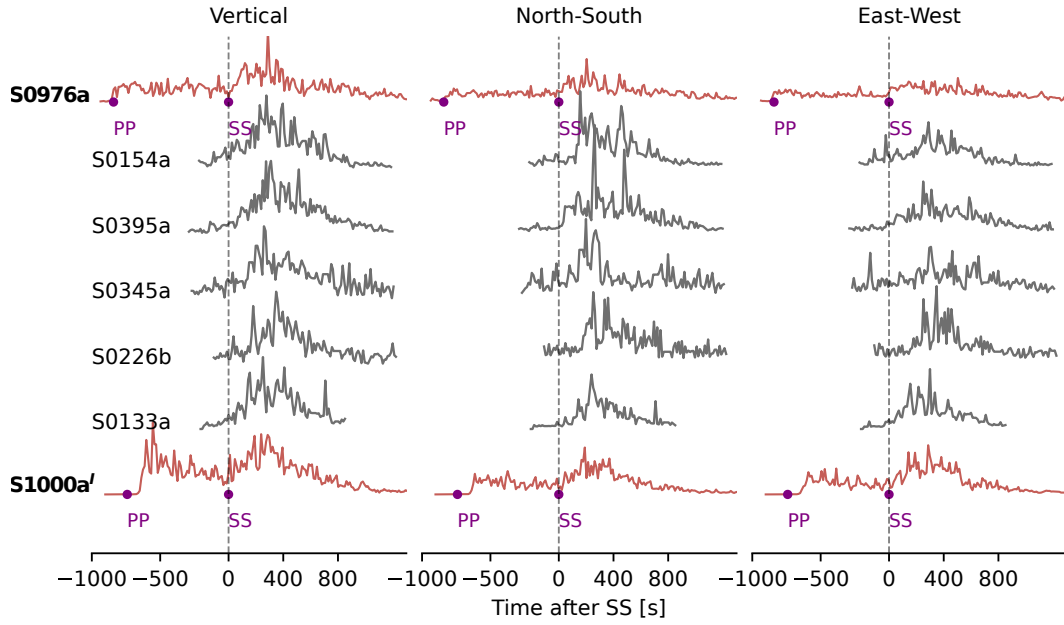


**Figure 7.** The class of most distant events, bound by the template events S0976a and S1000a<sup>T</sup> shown in red with bold font. The purple dots are the MQS phase picks used to determine distances for the templates. Time series show normalized vertical component envelopes. The template events are aligned on their SS phase picks. Other events are aligned with their energy onset which we interpret as S-waves.

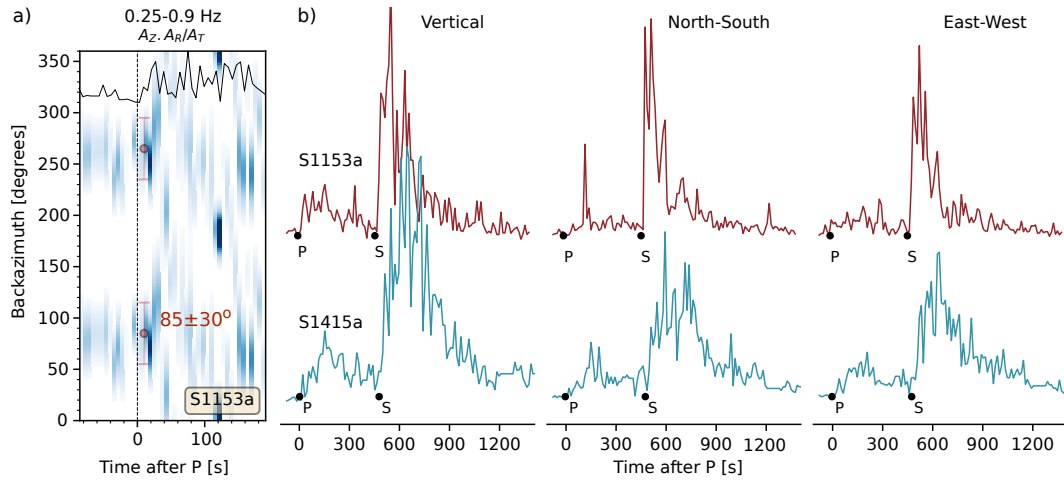


**Figure 8.** Backazimuth analysis and envelopes for the S1153a and S1415a event pair. (a) Backazimuth estimation for S1153a. (b) Three-component envelopes computed between 0.25–0.9 Hz using the VBB data in acceleration. Seismic phase picks from MQS are shown as black dots. The picking uncertainties for P and S are  $\pm 20$  and  $\pm 10$  s, respectively, for both events. See Figure S7c for the similarity warping path.

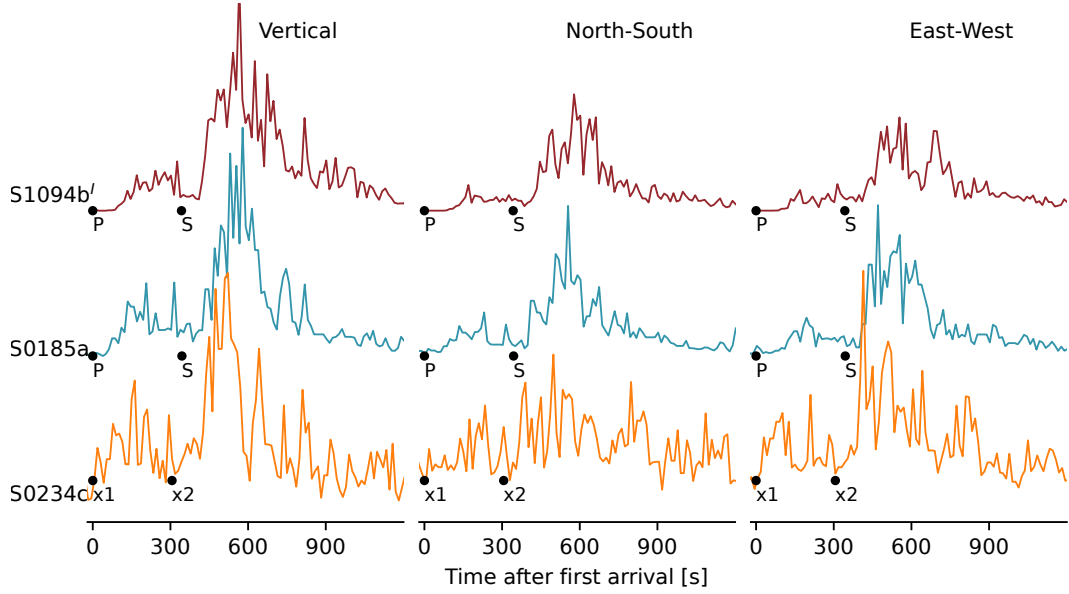


**Figure 9.** S1094b<sup>I</sup> class. The dots are the phase picks from the V14 catalog. MQS identified two phases for S0234c and labeled them as unknown (x1 and x2).

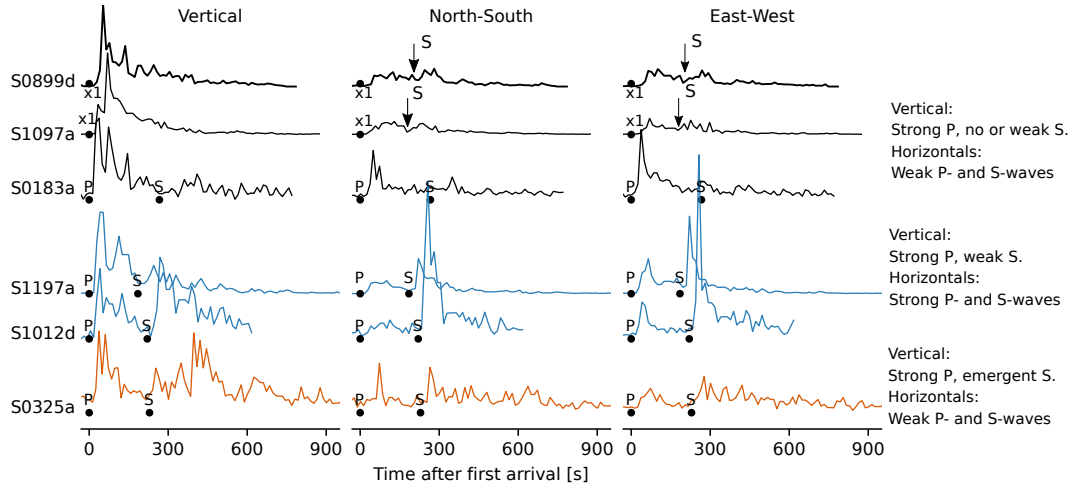


**Figure 10.** S0899d-like events with three sub-classes. MQS phase picks are denoted with dots. Only x1 picks were identified for S0899d and S1097a, though frequency-time domain polarisation analysis suggests these are P-wave energy. We propose new S-picks for both events using the horizontal components as shown with the down-pointing arrows.

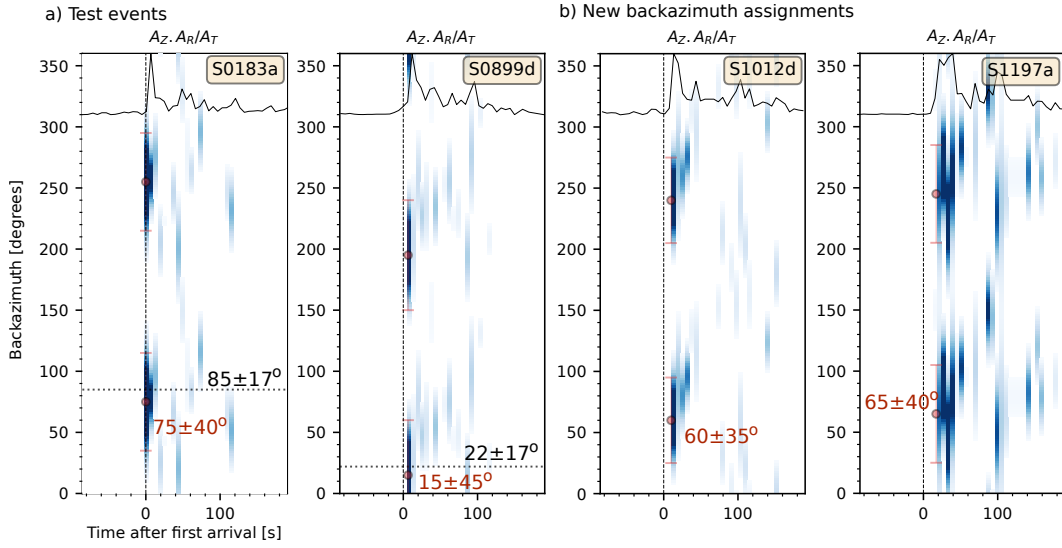


**Figure 11.** Envelope-based backazimuth estimates for S1012d and S1197a, events at similar distances to S0899d with weak or no S-waves. The dotted horizontal lines in (a) are the backazimuth values reported in the V14 catalog, while orange circles with error bars are our preferred backazimuth estimates. The similarity to the MQS values from V14 validates the grid search approach. (b) S1012d and S1197a are events without backazimuth estimates in V14. Other details follow Figure 4.

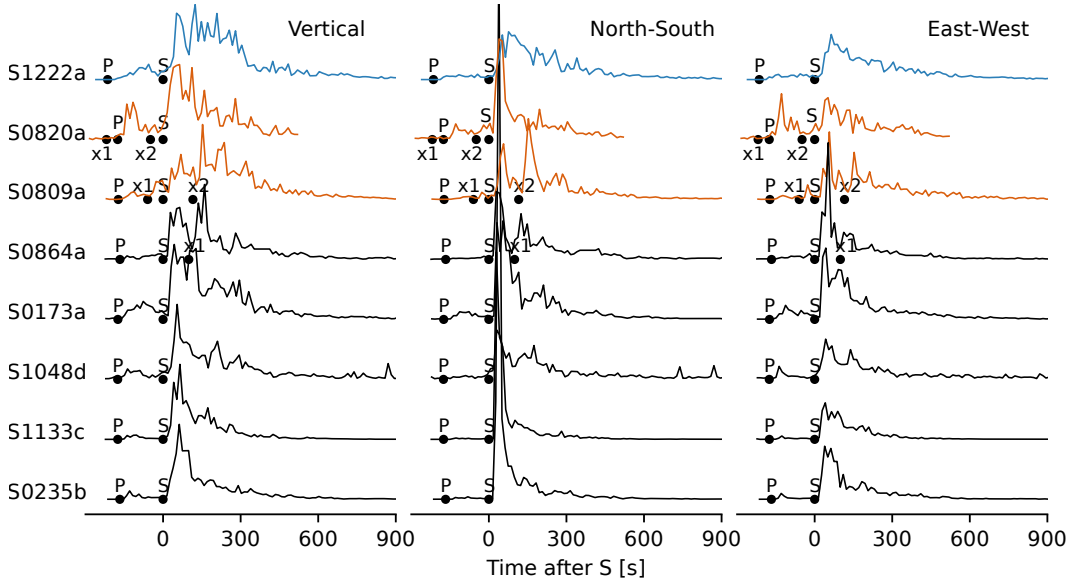


**Figure 12.** Three-component envelopes for S1222a and a subset of Cerberus Fossae events. The seismic phase picks from V14 are marked with dots. S0820a and S0809a (orange envelopes) are interpreted by MQS as double-events (Ceylan et al., 2022) with the additional phases marked as x1 and x2, instead of P and S, respectively.

## References

- Andrews-Hanna, J. C., Zuber, M. T., & Banerdt, W. B. (2008). The Borealis basin and the origin of the martian crustal dichotomy. *Nature*, *453*(7199), 1212–1215.
- Banerdt, W. B., Smrekar, S. E., Banfield, D., Giardini, D., Golombek, M., Johnson, C. L., ... Wieczorek, M. (2020). Initial results from the InSight mission on Mars. *Nat. Geosci.*, *13*(3), 183–189. doi: 10.1038/s41561-020-0544-y
- Banfield, D., Spiga, A., Newman, C., Forget, F., Lemmon, M., Lorenz, R., ... Banerdt, W. B. (2020, Mar 01). The atmosphere of mars as observed by insight. *Nature Geoscience*, *13*(3), 190–198. doi: 10.1038/s41561-020-0534-0
- Beghein, C., Li, J., Weidner, E., Maguire, R., Wookey, J., Lekić, V., ... Banerdt, W. (2022). Crustal anisotropy in the martian lowlands from surface waves. *Geophysical Research Letters*, *49*(24), e2022GL101508. doi: <https://doi.org/10.1029/2022GL101508>
- Böse, M., Clinton, J. F., Ceylan, S., Euchner, F., van Driel, M., Khan, A., ... Banerdt, W. B. (2017). A probabilistic framework for single-station location of seismicity on Earth and Mars. *Phys. Earth Planet. Inter.*, *262*, 48–65. doi: <https://doi.org/10.1016/j.pepi.2016.11.003>
- Böse, M., Giardini, D., Stähler, S., Ceylan, S., Clinton, J. F., van Driel, M., ... Banerdt, W. B. (2018). Magnitude Scales for Marsquakes. *Bull. Seismol. Soc. Am.*, *108*(5A), 2764–2777. doi: <https://doi.org/10.1785/0120180037>
- Byrne, P. K., Klimczak, C., Celâl Şengör, A. M., Solomon, S. C., Watters, T. R., & Hauck, S. A., II. (2014, Apr 01). Mercury’s global contraction much greater than earlier estimates. *Nature Geoscience*, *7*(4), 301–307. doi: 10.1038/ngeo2097
- Ceylan, S., Clinton, J. F., Giardini, D., Böse, M., Charalambous, C., van Driel, M., ... Perrin, C. (2021). Companion guide to the marsquake catalog from InSight, Sols 0–478: Data content and non-seismic events. *Phys. Earth Planet. Inter.*, *310*, 106597. doi: <https://doi.org/10.1016/j.pepi.2020.106597>
- Ceylan, S., Clinton, J. F., Giardini, D., Stähler, S. C., Horleston, A., Kawamura, T., ... Banerdt, W. B. (2022). The marsquake catalogue from InSight, sols 0–1011. *Phys. Earth Planet. Inter.*, 106943. doi: <https://doi.org/10.1016/j.pepi.2022.106943>
- Clinton, J., Ceylan, S., van Driel, M., Giardini, D., Stähler, S., Böse, M., ... Stott, A. (2021). The Marsquake catalogue from InSight, sols 0–478. *Phys. Earth Planet. Inter.*, *310*, 106595. doi: <https://doi.org/10.1016/j.pepi.2020.106595>
- Clinton, J., Giardini, D., Böse, M., Ceylan, S., van Driel, M., Euchner, F., ... Teanby, N. A. (2018). The marsquake service: Securing daily analysis of SEIS data and building the martian seismicity catalogue for InSight. *Space Sci. Rev.*, *214*(8).
- Coles, K. S., Tanaka, K. L., & Christensen, P. R. (2019). *The Atlas of Mars: Mapping its Geography and Geology*. Cambridge University Press. doi: 10.1017/9781139567428
- Daubar, I. J., Fernando, B., Garcia, R. F., & the InSight Impacts Working Group. (2023). InSight seismic events confirmed as impacts thus far. 2616, presented at the 54th Lunar and Planetary Science Conference, March 13–17, 2023.
- Durán, C., Khan, A., Ceylan, S., Charalambous, C., Kim, D., Drilleau, M., ... Giardini, D. (2022). Observation of a core-diffracted P-wave from a farside impact with implications for the lower-mantle structure of Mars. *Geophysical Research Letters*, *49*(21), e2022GL100887. doi: <https://doi.org/10.1029/2022GL100887>
- Durán, C., Khan, A., Ceylan, S., Zenhäusern, G., Stähler, S., Clinton, J., & Giardini, D. (2022). Seismology on mars: An analysis of direct, reflected, and converted seismic body waves with implications for interior structure. *Phys. Earth Planet. Inter.*, *325*, 106851. doi: <https://doi.org/10.1016/j.pepi.2022.106851>
- Garcia, R. F., Daubar, I. J., Beucler, É., Posiolova, L. V., Collins, G. S., Lognonné,

- P., ... Banerdt, W. B. (2022). Newly formed craters on Mars located using seismic and acoustic wave data from InSight. *Nat. Geosci.*, *15*(10), 774-780. doi: 10.1038/s41561-022-01014-0
- Giardini, D., Lognonné, P., Banerdt, W. B., Pike, W. T., Christensen, U., Ceylan, S., ... Yana, C. (2020). The Seismicity of Mars. *Nat. Geosci.* doi: 10.1038/s41561-020-0539-8
- Golombek, M. P., Banerdt, W. B., Tanaka, K. L., & Tralli, D. M. (1992). A prediction of Mars seismicity from surface faulting. *Science*, *258*(5084), 979-981. doi: 10.1126/science.258.5084.979
- Gudkova, T. V., Batov, A. V., & Zharkov, V. N. (2017, Nov 01). Model estimates of non-hydrostatic stresses in the Martian crust and mantle: 1—two-level model. *Solar System Research*, *51*(6), 457-478. doi: 10.1134/S003809461706003X
- Harris, C. R., Millman, K. J., van der Walt, S. J., Gommers, R., Virtanen, P., Cournapeau, D., ... Oliphant, T. E. (2020). Array programming with NumPy. *Nature*, *585*(7825), 357-362. doi: 10.1038/s41586-020-2649-2
- Horleston, A., Clinton, J., Ceylan, S., Giardini, D., Charalambous, C., Irving, J., ... Banerdt, W. (2022). The far side of Mars: two distant marsquakes detected by InSight. *The Seismic Record*. doi: 10.1785/0320220007
- InSight Mars SEIS Data Service. (2019a). *InSight SEIS Data Bundle. PDS Geosciences (GEO) Node*. doi: {10.17189/1517570}
- InSight Mars SEIS Data Service. (2019b). *SEIS raw data, InSight Mission. IPGP, JPL, CNES, ETHZ, ICL, MPS, ISAE-Supaero, LPG, MFSC*. doi: {10.18715/SEIS.INSIGHT.XB\\_2016}
- InSight Marsquake Service. (2020). *Mars Seismic Catalogue, InSight Mission; V3 2020-07-01*. ETHZ, IPGP, JPL, ICL, ISAE-Supaero, MPS, Univ. Bristol. Retrieved from <http://www.insight.ethz.ch/seismicity/catalog/v3> doi: 10.12686/a8
- InSight Marsquake Service. (2022). *Mars Seismic Catalogue, InSight Mission; V12 2022-10-01*. ETHZ, IPGP, JPL, ICL, Univ. Bristol. Retrieved from <https://www.insight.ethz.ch/seismicity/catalog/v12> doi: 10.12686/a18
- InSight Marsquake Service. (2023). *Mars Seismic Catalogue, InSight Mission; V14 2023-04-01*. ETHZ, IPGP, JPL, ICL, Univ. Bristol. Retrieved from <https://www.insight.ethz.ch/seismicity/catalog/v14> doi: 10.12686/a21
- Irving, J., Antonangeli, D., Banerdt, B., Li, J., Bozdog, E., Stähler, S., ... Stutzmann, E. (2022). First observations of seismic waves travelling through the martian core. DI44A-02, presented at 2022 AGU Fall Meeting, 12-16 December.
- Kawamura, T., Clinton, J. F., Zenhausern, G., Ceylan, S., Horleston, A. C., Dahmen, N. L., ... Banerdt, W. B. (2023). S1222a - the largest marsquake detected by InSight. *Geophysical Research Letters*, *50*(5), e2022GL101543. doi: <https://doi.org/10.1029/2022GL101543>
- Kedar, S., Panning, M. P., Smrekar, S. E., Stähler, S. C., King, S. D., Golombek, M. P., ... Banerdt, W. B. (2021). Analyzing low frequency seismic events at Cerberus Fossae as long period volcanic quakes. *Journal of Geophysical Research: Planets*, *126*(4), e2020JE006518. doi: <https://doi.org/10.1029/2020JE006518>
- Khan, A., Ceylan, S., van Driel, M., Giardini, D., Lognonné, P., Samuel, H., ... Banerdt, W. B. (2021). Upper mantle structure of Mars from InSight seismic data. *Science*, *373*(6553), 434-438. doi: 10.1126/science.abf2966
- Khan, A., Sossi, P., Liebske, C., Rivoldini, A., & Giardini, D. (2022). Geophysical and cosmochemical evidence for a volatile-rich Mars. *Earth and Planetary Science Letters*, *578*, 117330. doi: 10.1016/j.epsl.2021.117330
- Khan, A., van Driel, M., Böse, M., Giardini, D., Ceylan, S., Yan, J., ... Banerdt, W. B. (2016). Single-station and single-event marsquake location and inversion for structure using synthetic Martian waveforms. *Phys. Earth Planet. Inter.*

- 258, 28–42. doi: <https://doi.org/10.1016/j.pepi.2016.05.017>
- Kim, D., Banerdt, W., Ceylan, S., Giardini, D., Lekić, V., Lognonné, P., ... Panning, M. (2022). Surface waves and crustal structure on Mars. *Science*, 378(6618), 417–421. doi: 10.1126/science.abq7157
- Kim, D., Davis, P., Lekić, V., Maguire, R., Compaire, N., Schimmel, M., ... Banerdt, W. B. (2021). Potential pitfalls in the analysis and structural interpretation of seismic data from the Mars InSight mission. *Bull. Seismol. Soc. Am.*, 111(6), 2982–3002. doi: 10.1785/0120210123
- Kim, D., & et al. (2023). Global average crustal thickness revealed by surface waves orbiting Mars. *Geophysical Research Letters*, this issue(n/a), n/a. doi: n/a
- Kim, D., Lekic, V., Irving, J., Schmerr, N., Knapmeyer-Endrun, B., Joshi, R., ... Banerdt, W. (2021). Improving constraints on planetary interiors with PPs receiver functions. *Journal of Geophysical Research: Planets*, 126(11), e2021JE006983. doi: <https://doi.org/10.1029/2021JE006983>
- Kim, D., Stähler, S., Ceylan, S., Lekic, V., Maguire, R., Zenhäusern, G., ... Banerdt, W. B. (2023). Structure along the martian dichotomy constrained by rayleigh and love waves and their overtones. *Geophysical Research Letters*, n/a(n/a), e2022GL101666. doi: <https://doi.org/10.1029/2022GL101666>
- Knapmeyer, M., Oberst, J., Hauber, E., Wählisch, M., Deuchler, C., & Wagner, R. (2006). Working models for spatial distribution and level of mars' seismicity. *Journal of Geophysical Research: Planets*, 111(E11), E11006. doi: <https://doi.org/10.1029/2006JE002708>
- Knapmeyer, M., Stähler, S. C., Plesa, A.-C., Ceylan, S., Charalambous, C., Clinton, J., ... Banerdt, W. B. (2023). The global seismic moment rate of Mars after event S1222a. *Geophysical Research Letters*. doi: accepted
- Knapmeyer-Endrun, B., Panning, M. P., Bissig, F., Joshi, R., Khan, A., Kim, D., ... Banerdt, W. B. (2021). Thickness and structure of the martian crust from insight seismic data. *Science*, 373(6553), 438–443. doi: 10.1126/science.abf8966
- Krischer, L., Megies, T., Barsch, R., Beyreuther, M., Lecocq, T., Caudron, C., & Wassermann, J. (2015). ObsPy: a bridge for seismology into the scientific Python ecosystem. *Comput. Sci. Discov.*, 8(1), 014003.
- Li, J., Beghein, C., Wookey, J., Davis, P., Lognonné, P., Schimmel, M., ... Banerdt, W. B. (2022). Evidence for crustal seismic anisotropy at the insight lander site. *Earth and Planetary Science Letters*, 593, 117654. Retrieved from <https://www.sciencedirect.com/science/article/pii/S0012821X22002904> doi: <https://doi.org/10.1016/j.epsl.2022.117654>
- Lognonné, P., Banerdt, W., Giardini, D., Pike, W., Christensen, U., Laudet, P., ... Wookey, J. (2019). SEIS: Insight's Seismic Experiment for Internal Structure of Mars. *Space Sci. Rev.*, 215(1), 12. doi: 10.1007/s11214-018-0574-6
- Lognonné, P., Banerdt, W., Pike, W., Giardini, D., Christensen, U., Garcia, R., ... Zweifel, P. (2020). Constraints on the shallow elastic and anelastic structure of Mars from InSight seismic data. *Nat. Geosci.* doi: 10.1038/s41561-020-0536-y
- Perrin, C., Jacob, A., Lucas, A., Myhill, R., Hauber, E., Batov, A., ... Fuji, N. (2022). Geometry and segmentation of Cerberus Fossae, Mars: Implications for Marsquake properties. *Journal of Geophysical Research: Planets*, 127(1), e2021JE007118. doi: <https://doi.org/10.1029/2021JE007118>
- Posiolova, L. V., Lognonné, P., Banerdt, W. B., Clinton, J., Collins, G. S., Kawamura, T., ... Zenhäusern, G. (2022). Largest recent impact craters on Mars: Orbital imaging and surface seismic co-investigation. *Science*, 378(6618), 412–417. doi: 10.1126/science.abq7704
- Sakoe, H., & Chiba, S. (1978). Dynamic programming algorithm optimization for spoken word recognition. *IEEE Trans. Acoust.*, 26(1), 43–49. doi: 10.1109/TASSP.1978.1163055
- Scholz, J.-R., Widmer-Schmidrig, R., Davis, P., Lognonné, P., Pinot, B., Garcia,

- R. F., ... Banerdt, W. B. (2020). Detection, Analysis, and Removal of Glitches From InSight's Seismic Data From Mars. *Earth and Space Science*, 7(11), e2020EA001317. doi: <https://doi.org/10.1029/2020EA001317>
- Smith, D. E., Zuber, M. T., Frey, H. V., Garvin, J. B., Head, J. W., Muhleman, D. O., ... Sun, X. (2001). Mars Orbiter Laser Altimeter: Experiment summary after the first year of global mapping of Mars. *Journal of Geophysical Research: Planets*, 106(E10), 23689-23722. doi: <https://doi.org/10.1029/2000JE001364>
- Spohn, T., Hudson, T. L., Witte, L., Wippermann, T., Wisniewski, L., Kedziora, B., ... Grygorczuk, J. (2022, April). The InSight-HP3 mole on Mars: Lessons learned from attempts to penetrate to depth in the Martian soil. *Advances in Space Research*, 69(8), 3140–3163. doi: 10.1016/j.asr.2022.02.009
- Stähler, S. C., Khan, A., Banerdt, W. B., Lognonné, P., Giardini, D., Ceylan, S., ... Smrekar, S. E. (2021). Seismic detection of the martian core. *Science*, 373(6553), 443–448. doi: 10.1126/science.abi7730
- Stähler, S. C., Mittelholz, A., Perrin, C., Kawamura, T., Kim, D., Knapmeyer, M., ... Banerdt, W. B. (2022). Tectonics of cerberus fossae unveiled by marsquakes. *Nat. Astronomy*, 6(12), 1376-1386. doi: 10.1038/s41550-022-01803-y
- Tavenard, R., Faouzi, J., Vandewiele, G., Divo, F., Androz, G., Holtz, C., ... Woods, E. (2020). Tslern, a machine learning toolkit for time series data. *Journal of Machine Learning Research*, 21(118), 1-6. Retrieved from <http://jmlr.org/papers/v21/20-091.html>
- Virtanen, P., Gommers, R., Oliphant, T. E., Haberland, M., Reddy, T., Cournapeau, D., ... SciPy 1.0 Contributors (2020). SciPy 1.0: Fundamental Algorithms for Scientific Computing in Python. *Nature Methods*, 17, 261–272. doi: 10.1038/s41592-019-0686-2
- Weller, M. B. (2015). Basal Scarp (Olympus Mons, Mars). In H. Hargitai & Á. Kereszturi (Eds.), *Encyclopedia of Planetary Landforms* (pp. 137–141). New York, NY: Springer. doi: 10.1007/978-1-4614-3134-3\_14
- Zenhäusern, G., Stähler, S. C., Clinton, J. F., Giardini, D., Ceylan, S., & Garcia, R. F. (2022). Low-Frequency Marsquakes and Where to Find Them: Back Azimuth Determination Using a Polarization Analysis Approach. *Bull. Seismol. Soc. Am.*, 112(4), 1787-1805. doi: 10.1785/0120220019
- Zweifel, P., Mance, D., ten Pierick, J., Giardini, D., Schmelzbach, C., Haag, T., ... Banerdt, W. B. (2021, 10). Seismic High-Resolution Acquisition Electronics for the NASA InSight Mission on Mars. *Bull. Seismol. Soc. Am.*, 111(6), 2909-2923. doi: 10.1785/0120210071

# Supporting Information for “Mapping the seismicity of Mars with InSight”

S. Ceylan<sup>1</sup>, D. Giardini<sup>1</sup>, J. F. Clinton<sup>2</sup>, D. Kim<sup>1</sup>, A. Khan<sup>1,3</sup>, S. C. Stähler<sup>1,4</sup>, G. Zenhäusern<sup>1</sup>,  
P. Lognonné<sup>5</sup>, and W. B. Banerdt<sup>6</sup>

<sup>1</sup>Institute of Geophysics, ETH Zurich, Zurich, Switzerland

<sup>2</sup>Swiss Seismological Service, ETH Zurich, Zurich, Switzerland

<sup>3</sup>Institute of Geochemistry and Petrology, ETH Zurich, Zurich, Switzerland

<sup>4</sup>Physik-Institut, University of Zurich, Zurich, Switzerland

<sup>5</sup>Université Paris Cité, Institut de physique du globe de Paris, CNRS, Paris, France

<sup>6</sup>Jet Propulsion Laboratory, California Institute of Technology, Pasadena, CA, USA

## Contents of this file

1. Figures S1 to S12
2. Tables S1 and S2

## Introduction

In Table S1, we provide a breakdown of the V14 seismicity catalog from InSight (InSight Marsquake Service, 2023). Table S2 contains a list of re-evaluated events with a summary of modification proposed here. Figure S1 compares magnitude and distance distribution in V14 catalog and this study. The envelope computation steps and resulting cost matrix from similarity analysis are shown in Figure S2 and Figure S3, respectively. Figures S4–S6 demonstrate test cases for the backazimuth determination using grid search approach. Figure S7 show similarity analysis for 3 event classes. Figure S8 provides a summary of S1153a and S1415a. An additional comparison for S0235b and S0173a is provided in Figure S9. Interpretation and relocation of event classes are in Figures S10–S12.

**Table S1:** Breakdown of the MQS catalog V14 (InSight Marsquake Service, 2023). Events are classified into low-frequency (LF) and high-frequency (HF) families. The LF family is further classified into two types as LF and broadband (BB) events. The HF family consists of the 2.4 Hz, HF, very high-frequency (VF) sub-classes. Each event is cataloged with a quality identifier (QA being the highest quality and QD the most speculative) depending on the signal-to-noise ratio and reliability of phase picks. More information on the event classification is available in Clinton et al. (2021) and Ceylan et al. (2022). This study focuses on the LF family events only.

Event type	Total	QA	QB	QC	QD
<i>Low-frequency family</i>					
LF	59	6	12	20	21
BB	39	8	10	15	6
<i>High-frequency family</i>					
2.4Hz	989	–	50	353	586
HF	162	–	74	79	9
VF	74	–	29	34	11
<b>Total</b>	1319	14	175	500	630

**Table S2:** Breakdown of re-evaluated events and summary of the analysis done in this study.

Event name	Distance (°) in V14	Backazimuth (°) in V14	Distance (°) this study	Backazimuth (°) this study
<i>Cerberus Fossae events: 18 events. Re-located at the center of the Cerberus Fossae system, using the original distances as reported in V14.</i>				
S0105a	32.5±8.2	112±19	–	85±5
S0173a	30±1.4	88±11	–	85±5
S0235b	28.5±1.5	77±11	–	85±5
S0407a	29.3±2	90±62	–	85±5
S0474a	29.1±18	97±13	–	85±5
S0484b	31.8±5.9	100±20	–	85±5
S0784a	34.4±3.5	115±22	–	85±5
S0802a	30±3.5	82±15	–	85±5
S0809a	29.8±2	91±9	–	85±5
S0820a	30.2±2.4	106±17	–	85±5
S0864a	28.7±3.5	90±22	–	85±5
S0916d	29.3±5.9	97±36.5	–	85±5
S1015f	27.5±2	89±25	–	85±5
S1022a	30.7±2	63±5	–	85±5
S1048d	30.2±1.3	97±17	–	85±5
S1133c	30.2±1.3	91±14	–	85±5
<i>Events with weak or no S-wave: 4 events. New distances assigned to S0899d and S1097a. New backazimuth assigned to S1012d and S1197a, and combined with the previously reported distances, the events are now located.</i>				
S0899d	46.7±10*	22±30	32±10	–
S1197a	32.0±1.5	–	–	65±40
S1097a	46.2±10*	318±20	32±10	–
S1012d	38.2±3.3	–	–	60±35
<i>Events similar to S1094b<sup>l</sup>: 2 events. No modifications made.</i>				
S0185a	59.8±20	–	–	–
S0234c	–	–	60±20	–
<i>S1153a and S1415a: 2 events</i>				
<i>Backazimuth determined for S1153a. Both events are located SW of Olympus Mons.</i>				
S1153a	84.8±10	–	–	85±30
S1415a	88.2±9.6	–	–	85±30
<i>Distant cluster: 5 events. Distance assigned between 130–140°</i>				
<i>Located in the western Valles Marineris region using the S0976a backazimuth (101±25).</i>				
S0154a	–	–	130–140	101±25
S0395a	–	–	130–140	101±25
S0345a	–	–	130–140	101±25
S0226b	–	–	130–140	101±25
S0133a	–	–	130–140	101±25

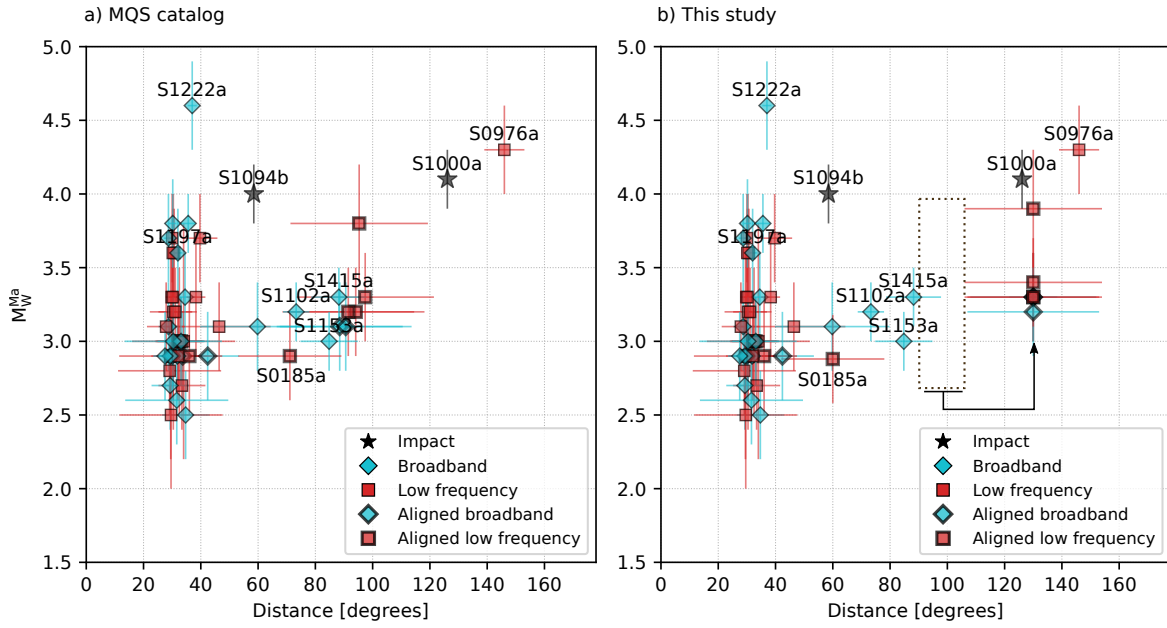


**Figure S1:** Distance vs Mars-calibrated moment magnitude ( $M_W^{\text{Ma}}$ ; Böse et al., 2018) distribution of the events (a) in the V14 MQS catalog and (b) after our interpretations in this study. The stars show the impacts. The distance values for the events with thicker symbol edges come from visual alignments.

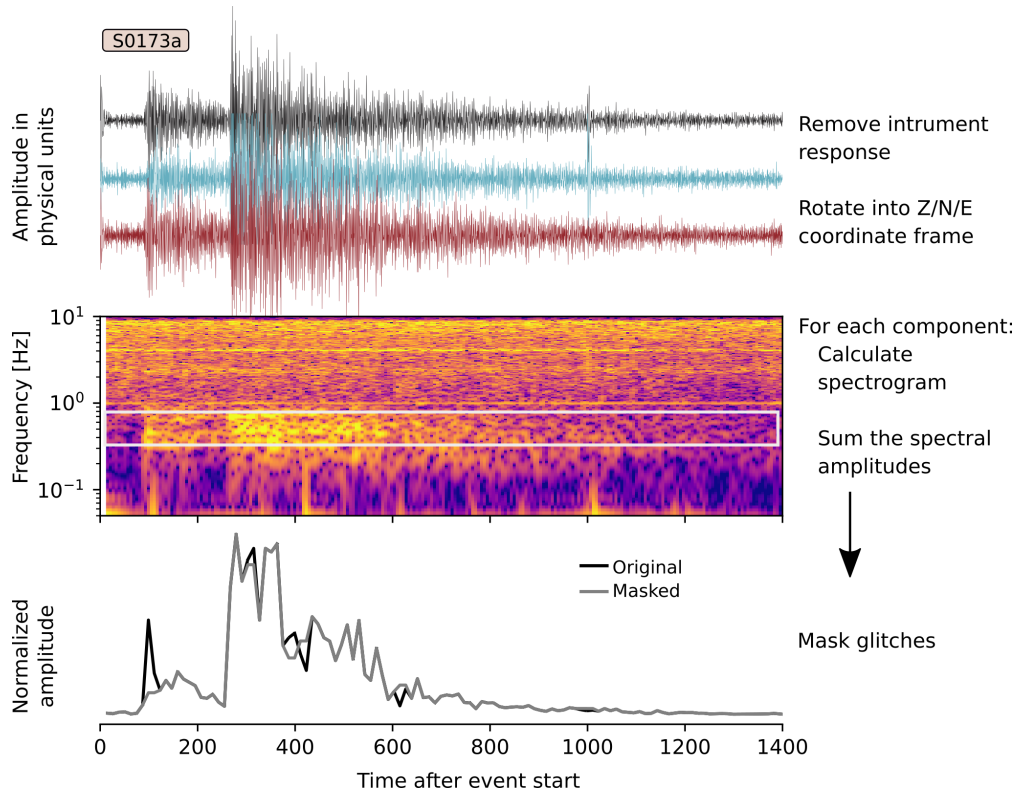


**Figure S2:** A sketch summarizing the envelope computation process using an example from S0173a (LF, quality A). The white rectangle in the middle panel represents the part of the spectrogram is used to create the envelope. Envelopes are computed by summing the spectral amplitudes along the frequency axis, then MQS-picked glitches are masked (bottom panel). These masked envelopes are used as input for the Dynamic Time Warping (DTW) (Sakoe and Chiba, 1978).

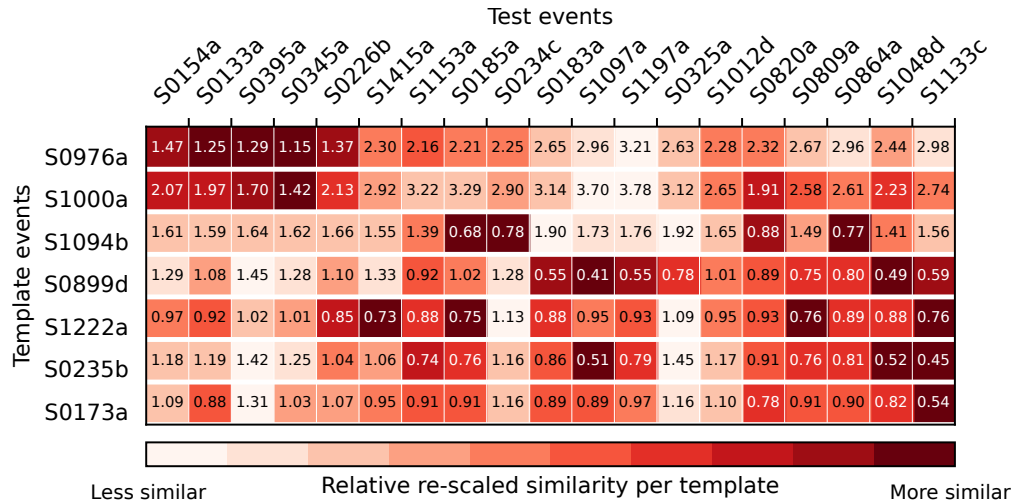


**Figure S3:** The cost matrix resulting from cross-similarity checks between the templates and test events discussed in this study. The DTW distances for event pairs are indicated in each cell. The colorbar shows the re-scaled relative similarity values per template event (rows) where lighter colors indicate less similarity.

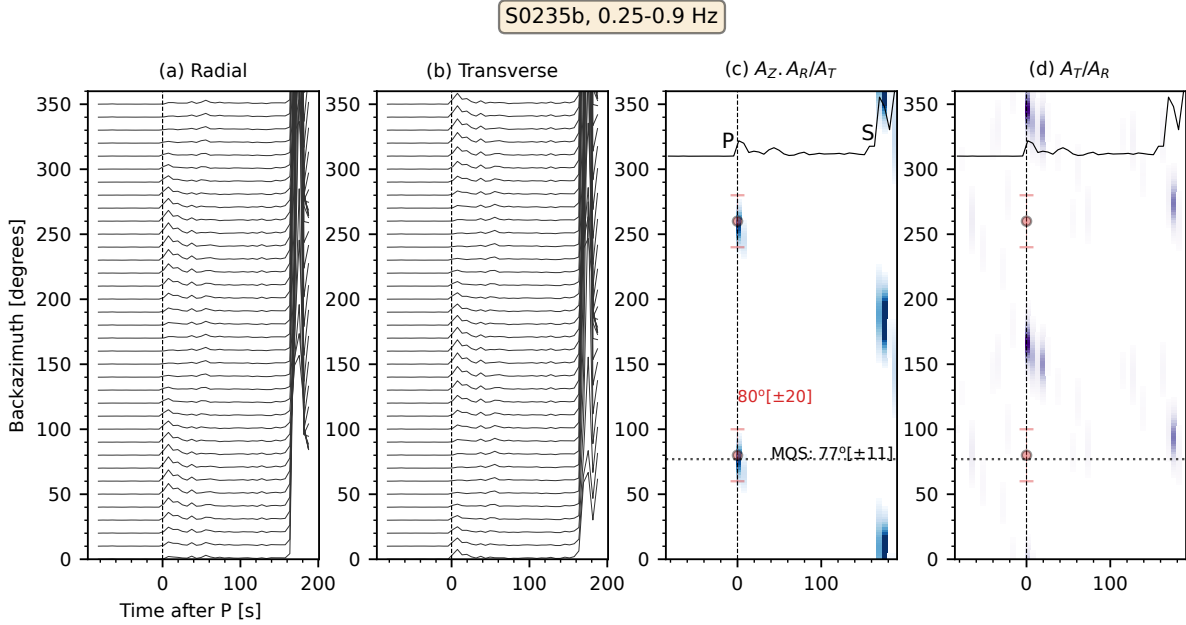


**Figure S4:** Test case for backazimuth estimation using our grid search approach for S0235b. The envelopes are computed for frequencies between 0.25 and 0.9 Hz. (a) and (b) show the rotated envelopes after normalization. (c) and (d) denote combined vertical (Z) and radial (R) to transverse (T) and T/R ratio, respectively. The estimated values from the grid search method and MQS are indicated. The orange dots with error bars show our preferred backazimuth pick, computed using envelope amplitudes before normalization. The envelopes for the vertical component are plotted at the top of (c) and (d) for reference.

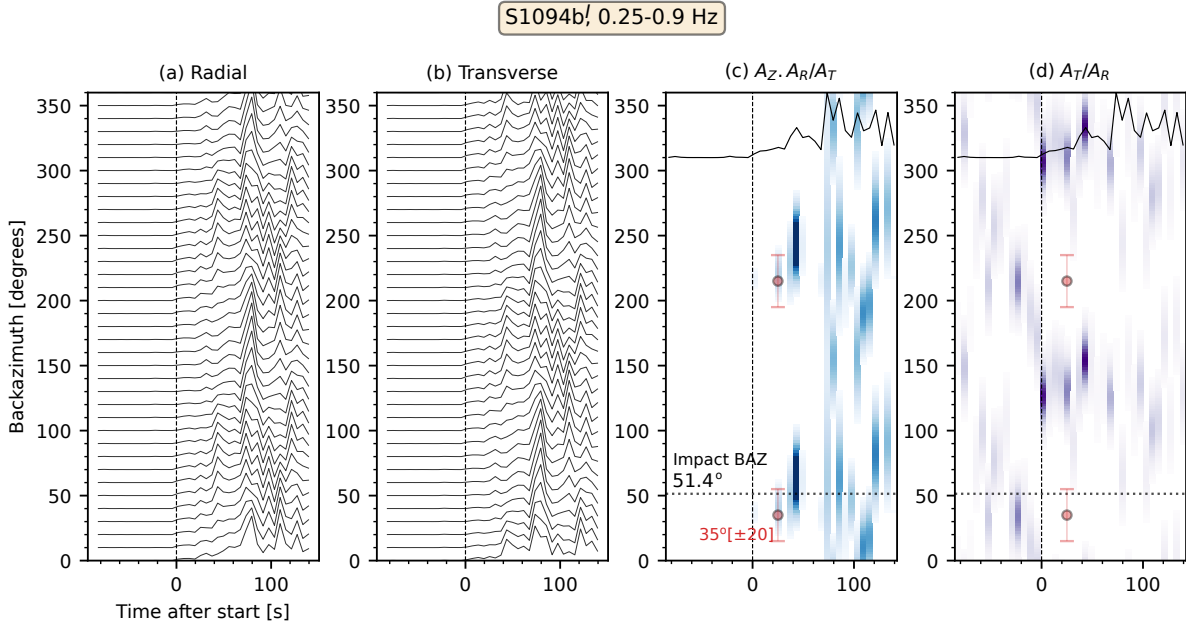


**Figure S5:** Backazimuth estimation for S1094b<sup>I</sup>. The true location is 58.5° away from InSight with a backazimuth of 51.4° (Posiolo et al., 2022). Other details follow Figure S4 caption.

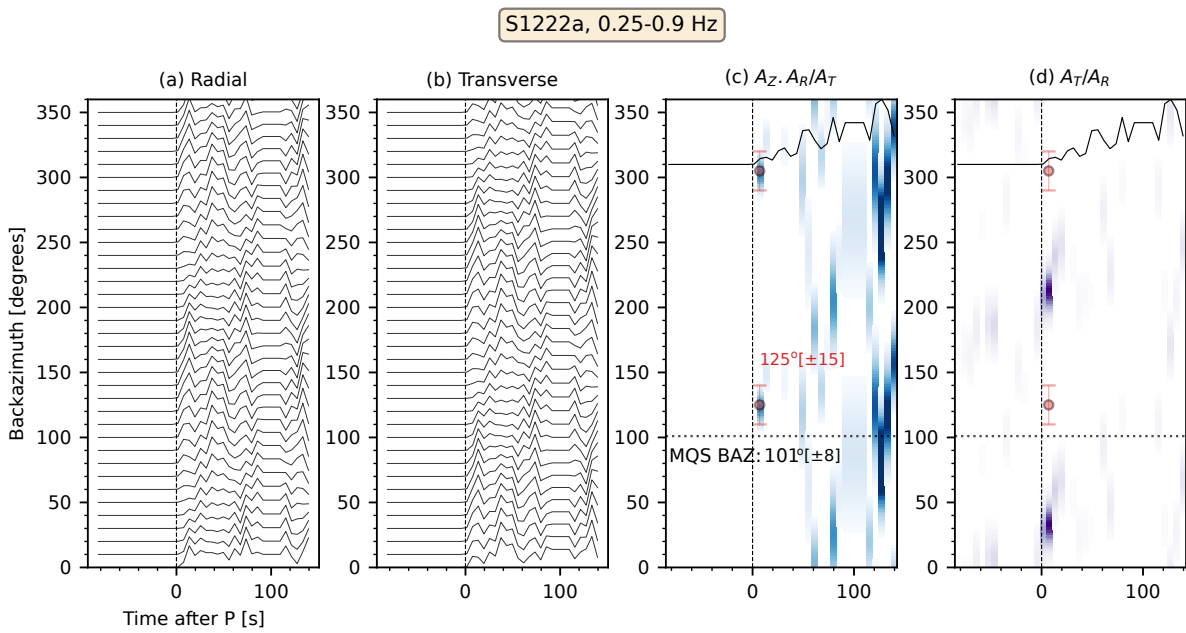


**Figure S6:** Test case for backazimuth estimation using S1222a. For this event, MQS computed a backazimuth of  $101 \pm 8^\circ$ . The figure caption follows Figure S4.

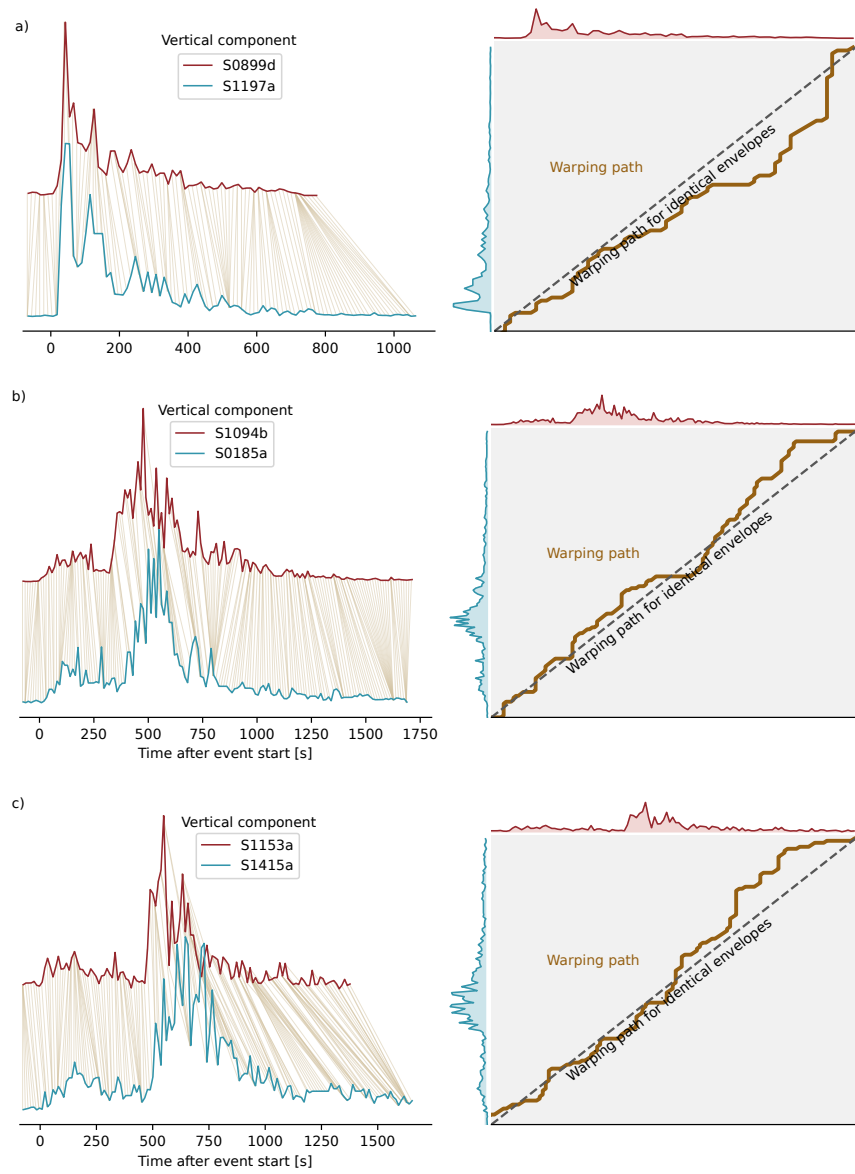


**Figure S7:** Warping path examples for 3 event classes. (a) S0899d and S1197a for weak-or-no S class, (b) S1094b<sup>I</sup> and S0185a for events similar to the impact, and (c) S1153a and S1415a event pair.

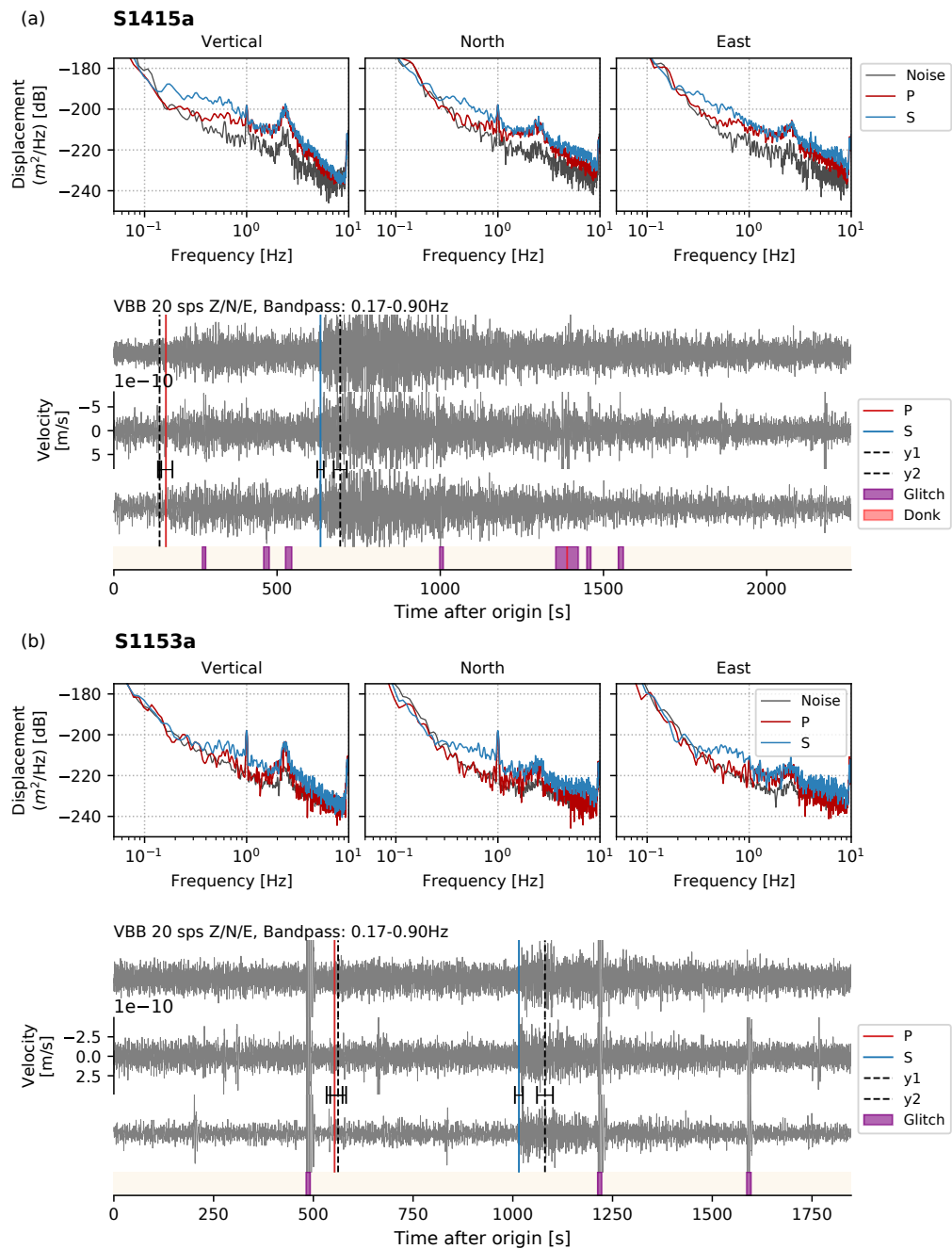


**Figure S8:** Event summary for S1415a (a) and S1153a (b), both broadband, quality B. Noise and signal windows in the displacement spectra are hand-picked by MQS. The seismic phases from MQS are shown with vertical lines with their picking uncertainties. The y1 and y2 phases (dashed lines) were picked on the high-frequency energy around 2.4 Hz.

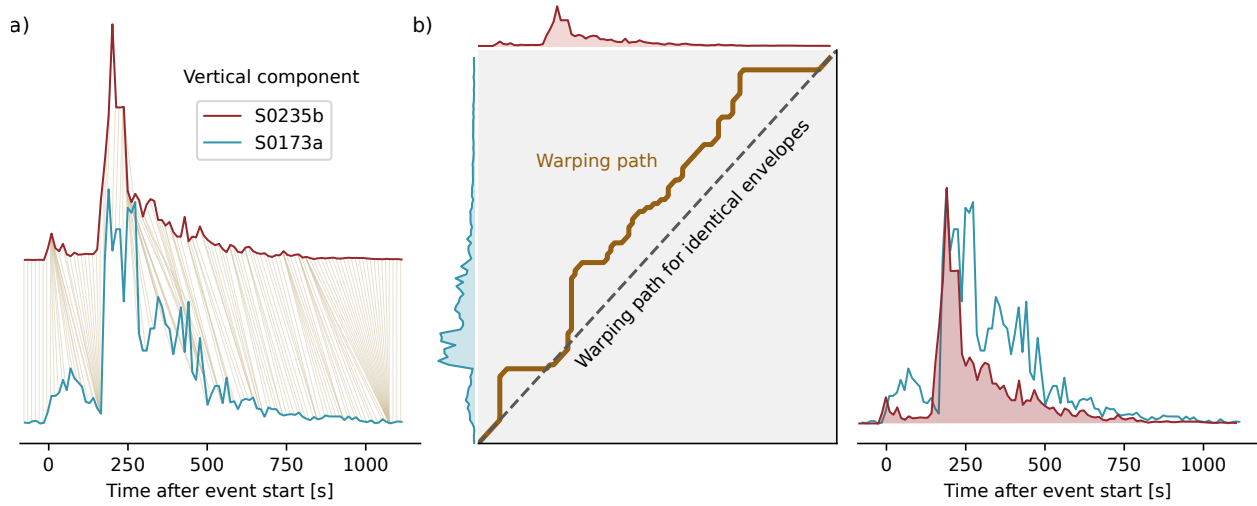


**Figure S9:** Comparison of S0235b and S0173a. (a) Point-wise warping match. (b) The warping path and envelopes in (a) overlapped. Note that the excess energy in the P- and S-coda makes similarity analysis harder although these two events originate from Cerberus Fossae and belong to the same class.

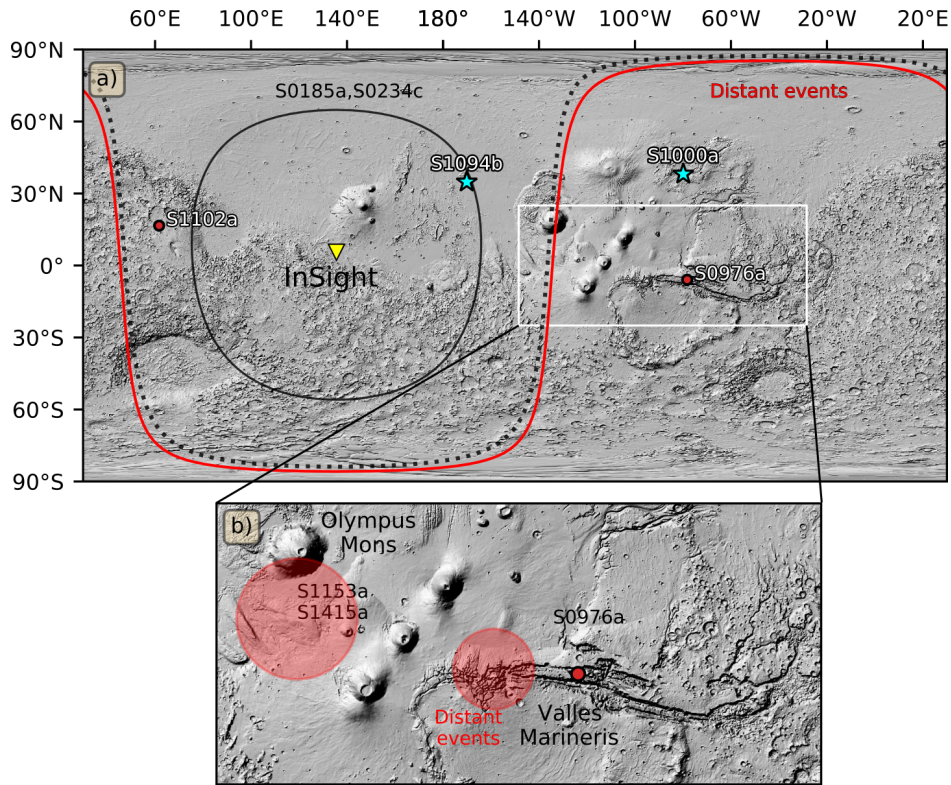


**Figure S10:** Interpretation of the events  $>60^\circ$ . In (a), we show the most recent understanding from MQS. The panel (b) shows our interpretation for these events, zooming around the Valles Marineris region. The locations of the two known impacts are marked as cyan stars. The distant events (red curve in (a)) are located at the western Valles Marineris region (labelled as distant events in (b)). MQS computed distances of S1153a and S1415a, but no backazimuth was provided. We propose a backazimuth of  $85 \pm 35^\circ$  for S1153a (dotted black line in (a)), and due to their similarity, locate the events in western Tharsis region at Olympus Mons.

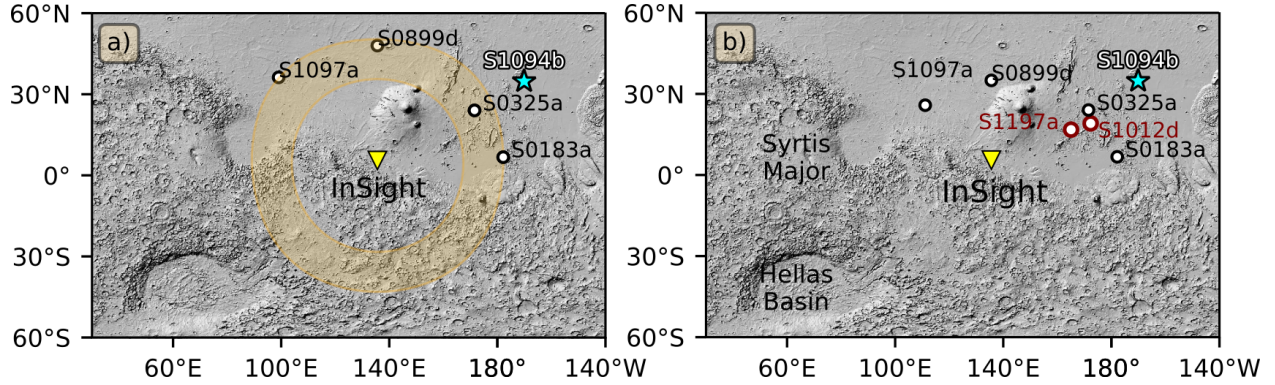


**Figure S11:** Interpretation of the events with no or weak S-wave energy. The template event is S0899d. (a) The current state in the MQS catalog (InSight Marsquake Service, 2023). The wheat-colored ring denotes the distance range ( $\sim 32\text{-}46^\circ$ ) which this class of events span. The S1094b<sup>I</sup> is shown with cyan star at  $58.5^\circ$  as a reference to distance ranges. (b) Our interpretation of event locations. We refrain the locations provided by MQS; in addition, we locate two more events (S1012d and S1197a) after our backazimuth analysis. We identify S-phases for S0899d and S1097a, and locate the events at  $31\text{-}32^\circ$  range.

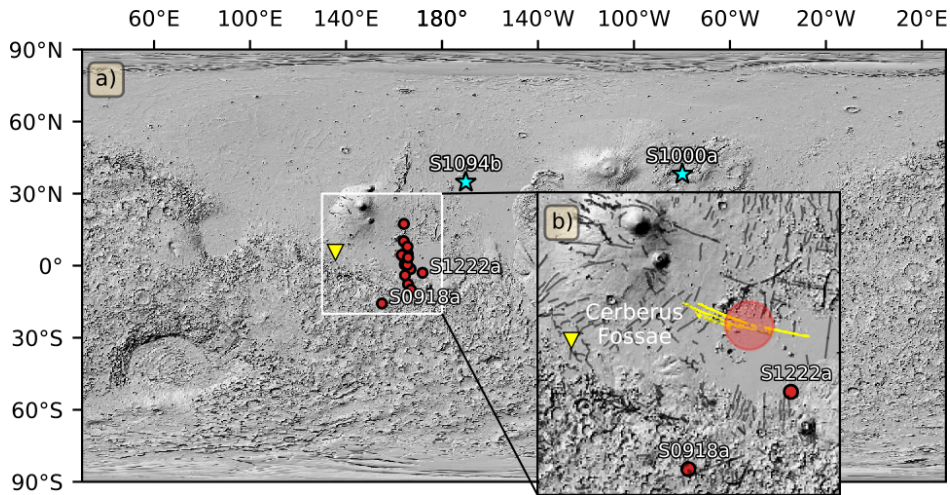


**Figure S12:** Interpretation of the events located in the Cerberus Fossae region. (a) Current MQS locations (red circles), and (b) our explanation of the seismicity. The faults in (b) are from Knappmeyer et al. (2006) and Perrin et al. (2022). The MQS event locations follow a North-South trend; however, the Cerberus fault system (yellow lines is (b) in NW-SE direction. Therefore, we project all events to the center. S1222a and S0918a are excluded due to their outlier locations.

## References

- Böse, M., D. Giardini, S. Stähler, S. Ceylan, J. F. Clinton, et al. (2018). “Magnitude Scales for Marsquakes”. In: *Bull. Seismol. Soc. Am.* 108.5A, pp. 2764–2777. ISSN: 0037-1106. DOI: <https://doi.org/10.1785/0120180037>.
- Ceylan, S., J. F. Clinton, D. Giardini, S. C. Stähler, A. Horleston, et al. (2022). “The marsquake catalogue from InSight, sols 0–1011”. In: *Phys. Earth Planet. Inter.*, p. 106943. DOI: <https://doi.org/10.1016/j.pepi.2022.106943>.
- Clinton, J., S. Ceylan, M. van Driel, D. Giardini, S. Stähler, et al. (2021). “The Marsquake catalogue from InSight, sols 0–478”. In: *Phys. Earth Planet. Inter.* 310, p. 106595. ISSN: 0031-9201. DOI: <https://doi.org/10.1016/j.pepi.2020.106595>.
- InSight Marsquake Service (2023). *Mars Seismic Catalogue, InSight Mission; V14 2023-04-01*. en. DOI: 10.12686/a21. URL: <https://www.insight.ethz.ch/seismicity/catalog/v14>.
- Knapmeyer, M., J. Oberst, E. Hauber, M. Wählisch, C. Deuchler, and R. Wagner (2006). “Working models for spatial distribution and level of Mars’ seismicity”. In: *Journal of Geophysical Research: Planets* 111.E11, E11006. DOI: <https://doi.org/10.1029/2006JE002708>.
- Perrin, C., A. Jacob, A. Lucas, R. Myhill, E. Hauber, et al. (2022). “Geometry and segmentation of Cerberus Fossae, Mars: Implications for Marsquake properties”. In: *Journal of Geophysical Research: Planets* 127.1, e2021JE007118. DOI: <https://doi.org/10.1029/2021JE007118>.
- Posiolova, L. V., P. Lognonné, W. B. Banerdt, J. Clinton, G. S. Collins, et al. (2022). “Largest recent impact craters on Mars: Orbital imaging and surface seismic co-investigation”. In: *Science* 378.6618, pp. 412–417. DOI: 10.1126/science.abq7704.
- Sakoe, H. and S. Chiba (1978). “Dynamic programming algorithm optimization for spoken word recognition”. In: *IEEE Trans. Acoust.* 26.1, pp. 43–49. DOI: 10.1109/TASSP.1978.1163055.